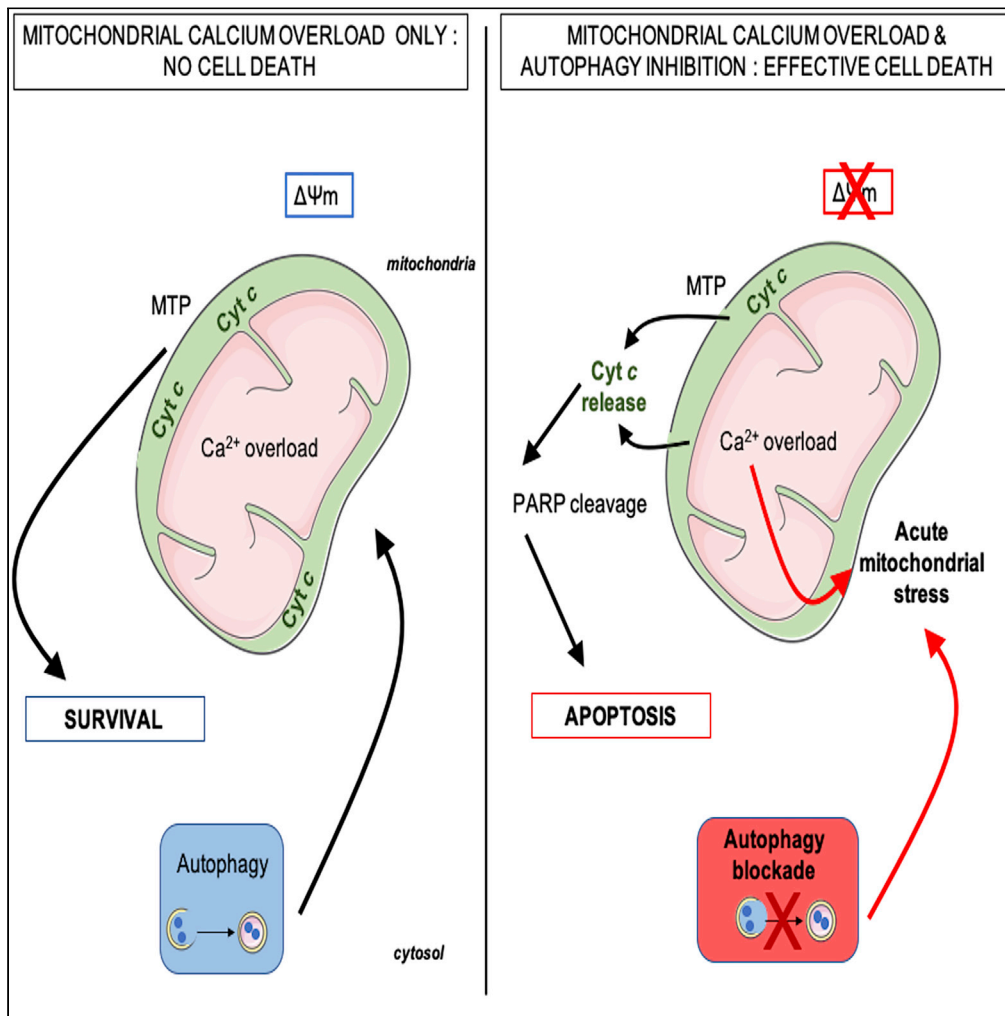


Article

# Co-targeting Mitochondrial Ca<sup>2+</sup> Homeostasis and Autophagy Enhances Cancer Cells' Chemosensitivity



Charlotte Dubois,  
Artem  
Kondratskyi,  
Gabriel Bidaux, ...,  
Jean-Louis  
Bonnal, Natalia  
Prevarskaya,  
Fabien Vanden  
Abeelee

charlotte.dubois@inserm.fr  
(C.D.)  
fabien.vanden-abeelee@  
inserm.fr (F.V.A.)

**HIGHLIGHTS**

Mitochondrial Ca<sup>2+</sup>  
overload stimulus alone is  
ineffective to induce cell  
death

Autophagy is a  
gatekeeper of cell fate in  
response to Ca<sup>2+</sup>  
homeostasis disruption

Mitochondrial Ca<sup>2+</sup>  
overload is a determinant  
of autophagy as a  
chemosensitizer



## Article

Co-targeting Mitochondrial Ca<sup>2+</sup> Homeostasis and Autophagy Enhances Cancer Cells' Chemosensitivity

Charlotte Dubois,<sup>1,\*</sup> Artem Kondratskiy,<sup>1</sup> Gabriel Bidaux,<sup>2,3</sup> Lucile Noyer,<sup>1</sup> Eric Vancauwenberghe,<sup>4</sup> Valério Farfariello,<sup>1</sup> Robert-Allain Toillon,<sup>5</sup> Morad Roudbaraki,<sup>1</sup> Dominique Tierny,<sup>6</sup> Jean-Louis Bonnal,<sup>1,7</sup> Natalia Prevarskaya,<sup>1</sup> and Fabien Vanden Abeele<sup>1,8,\*</sup>

## SUMMARY

**Mitochondria are important cell death checkpoints, and mitochondrial Ca<sup>2+</sup> overload is considered as a potent apoptotic intrinsic pathway inducer. Here, we report that this Ca<sup>2+</sup> apoptosis link is largely ineffective in inducing cell-death just by itself and required a concomitant inhibition of autophagy to counteract its pro-survival action. In such condition, an acute mitochondrial stress revealed by a DRP1-mediated mitochondrial dynamic remodeling is observed concomitantly with mitochondrial depolarization, release of cytochrome c, and efficient apoptosis induction. We also uncover that mitochondrial Ca<sup>2+</sup> status modulates the function of autophagy as a sensitizer for chemotherapies. This priming mediated by mitochondrial Ca<sup>2+</sup> overload and inhibition of autophagy sensitizes many cancer cells types to different chemotherapies with independent mechanisms of action. Collectively, our results redefine an important cell signaling pathway, uncovering new combined therapies for the treatment of diseases associated with mitochondrial Ca<sup>2+</sup> homeostasis disorders such as cancer.**

## INTRODUCTION

Calcium (Ca<sup>2+</sup>) is a critical intracellular second messenger, which controls key cell fate decisions, such as metabolism, proliferation, or apoptosis (Rossi et al., 2019). Specific Ca<sup>2+</sup> signaling pathways have long been known to play an important role in apoptosis induction and/or regulation, which occurs through endoplasmic reticulum (ER) Ca<sup>2+</sup> stress, and cytosolic and mitochondrial Ca<sup>2+</sup> overload (Berridge et al., 2000; Orrenius et al., 2003; Pinton et al., 2008). Each of these pathways has been associated alone or in combination with apoptosis induction or resistance, both in physiological and physiopathological conditions. Indeed, the ER lumen is the major storage of intracellular Ca<sup>2+</sup>, allowing the proper folding of proteins by Ca<sup>2+</sup>-binding chaperones (Wang and Kaufman, 2014). Depletion of ER Ca<sup>2+</sup> stores is considered to be a robust stress condition that triggers cell death (Giorgi et al., 2010; Prevarskaya et al., 2004). Other studies have also demonstrated that a large and sustained elevation of cytosolic Ca<sup>2+</sup> concentration ([Ca<sup>2+</sup>]<sub>c</sub>) is another key process for triggering apoptosis, mainly induced by store-operated Ca<sup>2+</sup> entry (Vanden Abeele et al., 2002; Prevarskaya et al., 2010). Finally, mitochondrial Ca<sup>2+</sup> overload resulting from sustained elevation of [Ca<sup>2+</sup>]<sub>c</sub> is considered to be one of the ways to induce mitochondrial-mediated intrinsic apoptotic pathway (Berridge et al., 2000; Orrenius et al., 2003; Pinton et al., 2008; Zhivotovsky and Orrenius, 2011). The crucial factor is the magnitude of the Ca<sup>2+</sup> signal received by the mitochondria. A high Ca<sup>2+</sup> load will lead to the mitochondrial permeability transition pore (MPTP) (Lemasters et al., 2009) and eventually to the permeabilization of the outer mitochondrial membrane (OMM). As a consequence, targeting mitochondria and in particular mitochondrial Ca<sup>2+</sup> homeostasis to sensitize cancer cells to apoptosis and to overcome drug resistance represents a major aim in anti-cancer therapy (Wen et al., 2013; Zhang et al., 2016).

However, the expected role of Ca<sup>2+</sup> could be less clear than it was first proposed. Indeed, we have identified in a previous study that a potent Ca<sup>2+</sup> homeostasis disruption characterized by a sustained increase of cytosolic Ca<sup>2+</sup> and ER Ca<sup>2+</sup> stress is not sufficient enough to induce apoptosis (Dubois et al., 2013). However, the role of mitochondria was not investigated, and more importantly the molecular mechanisms

<sup>1</sup>Univ. Lille, Inserm, U1003 - PHYCEL – Physiologie Cellulaire, 59000 Lille, France

<sup>2</sup>Univ Lyon, CarMeN Laboratory, INSERM, INRA, INSA Lyon, Université, Claude Bernard Lyon 1, 69550 Bron, France

<sup>3</sup>Hospices Civils de Lyon, Groupement Hospitalier EST, Département de Cardiologie, IHU-OPERA Bâtiment B13, 69550 Bron, France

<sup>4</sup>Nottingham Breast Cancer Research, Centre Hypoxia and Tumour Microenvironment Group Cancer Biology, Division of Cancer and Stem Cells School of Medicine, Queen's Medical Centre, Nottingham NG7 2UH, UK

<sup>5</sup>Univ. Lille, Inserm, U908, 59000 Lille, France

<sup>6</sup>Oncovet Clinical Research, SIRIC ONCOLILLE, 80 Rue du Dr Yersin, 59120 Loos, France

<sup>7</sup>Service d'Urologie de l'hôpital St-Philibert, Lomme, France

<sup>8</sup>Lead Contact

\*Correspondence: charlotte.dubois@inserm.fr (C.D.), fabien.vanden-abeele@inserm.fr (F.V.A.)

<https://doi.org/10.1016/j.isci.2020.101263>



underlying this atypical mode to escape from cell death were not identified. Moreover, an increasing number of studies have demonstrated that  $\text{Ca}^{2+}$  also plays an important role in the regulation of more recent hallmark of cancer, such as autophagy involved in tumor development and cancer therapy (Degenhardt et al., 2006; Hanahan and Weinberg, 2011; Yang et al., 2011). Autophagy is a catabolic degradation process in which cellular proteins and organelles are enveloped by double-membrane autophagosomes and degraded in lysosomes (Chen and Klionsky, 2011; Ravikumar et al., 2010). The autophagic process attempts to restore metabolic homeostasis, and the current consensus is that autophagy has a dual role in cancer (Jiang et al., 2015; Kroemer, 2015; White, 2015). During the early steps of cancer development, autophagy functions as a tumor suppressor mechanism by preventing the accumulation of damaged organelles and aggregated proteins. In contrast, autophagy is considered as a pro-survival mechanism for established tumors in response to metabolic stresses such as nutrient deprivation, hypoxia, and absence of growth factors. Autophagy has also emerged as a crucial player in drug resistance in response to chemotherapies (Kroemer, 2015). Importantly, autophagy is shown to precede or to act in parallel with apoptosis process, but the precise molecular mechanisms involved are still not fully understood (Sui et al., 2013) and in particular the role of autophagy in cell death mediated by  $\text{Ca}^{2+}$  homeostasis disruption is not fully understood. Finally, it has been also reported that some  $\text{Ca}^{2+}$  signaling pathways and  $\text{Ca}^{2+}$  modulators used to depict apoptotic pathways have also significant implications in other signaling pathways such as autophagy, highlighting the need of better tools (Bootman et al., 2018; Dubois et al., 2016).

Here, we dissect the interplay between survival pathways such as autophagy and mitochondrial dynamics to establish their precise role(s) in cell death mediated by  $\text{Ca}^{2+}$  homeostasis disruption. Collectively, our results challenge a crucial paradigm in cell death and provide new concepts for more rational approaches in cancer treatments. Indeed, we propose an effective combined strategy based on concomitant mitochondrial  $\text{Ca}^{2+}$  overload and autophagy inhibition with drugs in clinical evaluation to increase the sensitivity of chemotherapies in most common cancer types.

## RESULTS

### $\text{Ca}^{2+}$ Homeostasis Perturbations *per se* Are Not Sufficient to Induce Apoptotic Cell Death

To investigate the role of  $\text{Ca}^{2+}$  homeostasis perturbations in apoptosis induction, we performed an in-depth study by using several sarcoplasmic ER  $\text{Ca}^{2+}$  ATPase (SERCA) inhibitors (thapsigargin [TG], TG analogs, and cyclopiazonic acid [CPA]). SERCA resides in the ER and plays a crucial role in maintaining cellular  $\text{Ca}^{2+}$  homeostasis (Berridge et al., 2000; Orrenius et al., 2003; Pinton et al., 2008). We used concentrations of SERCA inhibitors known to induce a robust disruption of  $\text{Ca}^{2+}$  homeostasis (Quynh Doan and Christensen, 2015). The TG analogs tested were ASP-8ADT (also known as 12-ADT-ASP), EPO-8ADT, and LEU-8ADT, and all of them have been characterized in cell-free system for their specific activity on SERCA pumps and functionally on several cell types (Jakobsen et al., 2001). As we have already demonstrated (Dubois et al., 2013), all analogs were able to induce an influx of  $\text{Ca}^{2+}$  across the plasma membrane due to the activation of SOC (store-operated channel) in response to ER  $\text{Ca}^{2+}$  store depletion triggered by SERCA inhibition (Figure 1A). Here, we therefore evaluated their ability to maintain high cytosolic  $\text{Ca}^{2+}$  concentration ( $[\text{Ca}^{2+}]_c$ ) over a longer period of time, which has been also associated with apoptosis induction (Figure 1B) (Berridge et al., 2003; Clapham, 2007). We observed that only TG, ASP-8ADT, and LEU-8ADT (1  $\mu\text{M}/18$  h) were able to induce a sustained  $[\text{Ca}^{2+}]_c$  increase compared with EPO-8ADT or CPA (1  $\mu\text{M}/18$  h) (Figure 1B). In accordance, these discrepancies may have significant consequences on mitochondrial  $\text{Ca}^{2+}$  contents, as it is largely accepted that sustained  $\text{Ca}^{2+}$  entry is also a major factor in the process of mitochondrial  $\text{Ca}^{2+}$  overload (Berridge et al., 2000; Orrenius et al., 2003; Pinton et al., 2008; Zhivotovsky and Orrenius, 2011). Thus, we evaluated the extent of mitochondrial  $\text{Ca}^{2+}$  overload following the same setting of treatment. We observed that only TG, ASP-8ADT, and LEU-8ADT induced mitochondrial  $\text{Ca}^{2+}$  overload in prostate cancer cell lines (Figures 1C and 1D) and five additional cancer cell lines (Figure S1). In parallel, we correlated the ability of these compounds to induce  $\text{Ca}^{2+}$ -mediated apoptosis in prostate (Figures 1E–1H), breast (Figure 1I), and pancreatic cancer cells (Figures 1J and S1A–S1O). Surprisingly, only TG and LEU-8ADT were potent apoptosis inducers in all cell lines. Both compounds have a similar ability to induce mitochondrial  $\text{Ca}^{2+}$  overload and to maintain high  $[\text{Ca}^{2+}]_c$  over a longer period (Figure 1B). However, LEU-8ADT induced a slower initial  $\text{Ca}^{2+}$  influx rate compared with TG (Figure 1A). Conversely, the initial  $\text{Ca}^{2+}$  influx rate was higher for ASP-8ADT compared with LEU-8ADT despite its low efficiency in inducing cell death. This implies that the initial  $\text{Ca}^{2+}$  influx was not correlated with the induction of apoptosis. Concerning TG and ASP-8ADT, whereas the remodeling on  $\text{Ca}^{2+}$  homeostasis was quite similar, compared with TG, apoptosis induced by ASP-8ADT was very modest particularly in the LNCaP or PC-3 prostate cancer cell

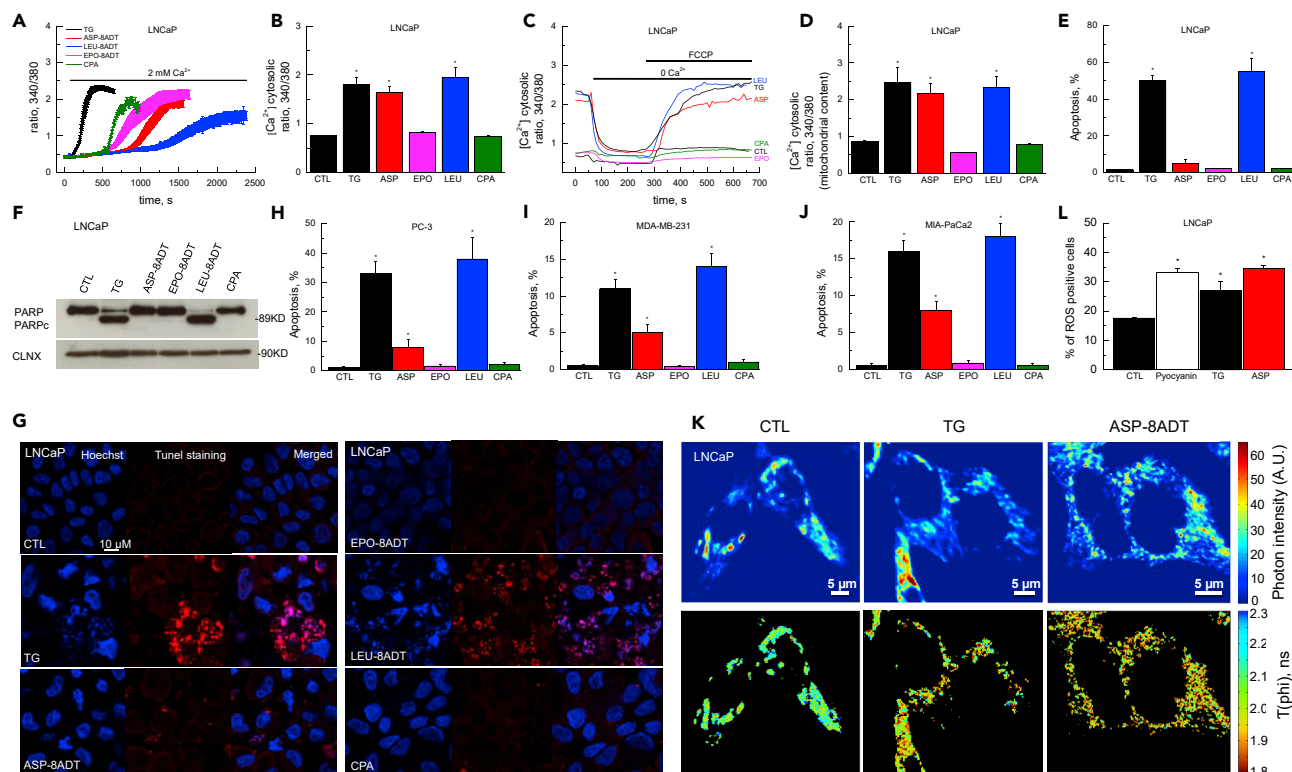


### Figure 1. Redefining the $Ca^{2+}$ -Apoptosis Link

(A) Representative measurements of SOCE activated by SERCA pump inhibitors (TG; TG analogs: ASP-8ADT, LEU-8ADT, EPO-8ADT; CPA), as indicated by  $[Ca^{2+}]_c$  elevation in LNCaP cells.

(B) Quantification of  $[Ca^{2+}]_c$  in LNCaP cells subjected or not to cytosolic  $Ca^{2+}$  overload 18 h after SERCA pump inhibitor treatment.

(C) Representative recordings of FCCP-induced  $[Ca^{2+}]_c$  elevation in LNCaP cells subjected or not to mitochondrial  $Ca^{2+}$  overload 18 h after SERCA pump inhibitor treatment.

(D) Quantification of the results presented in (C).

(E) Quantification of apoptotic cells, as determined by Hoechst staining, 48 h after treatment with the control or the indicated drug (TG, 1  $\mu$ M; ASP-8ADT, 1  $\mu$ M; EPO-8ADT, 1  $\mu$ M; LEU-8ADT, 1  $\mu$ M and CPA, 10  $\mu$ M).

(F) Representative western blot of the apoptosis marker protein PARP in LNCaP cells 24 h after treatment with control or the indicated drug as in (E). Data are representative of 3 independent experiments.

(G) TUNEL staining of LNCaP cells 18 h after treatment.

(H–J) Quantification of apoptotic cells, as determined by manual counting of condensed nuclei following Hoechst staining, 48 h after treatment with control or the indicated drug in PC-3 (prostate), MDA-MB-231 (breast), and MIA-PaCa2 (pancreatic) cancer cells.

(K) Photon intensity (top) and phase lifetime (down),  $\tau(\text{phi})$ , of Cerulean fluorescent protein encoded in the mitochondria-target Cameleon biosensor, 4mtTM3cpv, expressed in LNCaP cells for 36 h. Cells were incubated with either TG or ASP-8ADT compounds for 24 h before performing TD-FLIM experiment. Experiments were performed twice independently, and 15 cells were analyzed per experiment.

(L) Quantification of ROS production using flow cytometry 18 h of treatment with TG (1  $\mu$ M) and ASP-8ADT (1  $\mu$ M). Pyocyanin (100  $\mu$ M/30 min) is used as an ROS inducer. Oxidative Stress Detection Reagent (green fluorescent) for total ROS detection is used (ENZO LIFE SCIENCES). Experiments performed in triplicate. Bars represent mean  $\pm$  SEM. \* $p < 0.05$ , Student's t test, when compared with corresponding control.

lines. These results were unexpected as they are not in line with the commonly established key role of mitochondrial  $Ca^{2+}$  overload in the process of apoptosis induction. Thus, we decided to confirm that ASP-8ADT was able to induce mitochondrial  $Ca^{2+}$  overload by using two other independent approaches that allow a direct assessment of  $Ca^{2+}$  handling by mitochondria. By measuring steady-state  $Ca^{2+}$  concentration in mitochondria with the 4mtD3cpv biosensor or with the ratiometric genetically encoded  $Ca^{2+}$  probe mito-GEM-GECO1, we confirmed that TG and ASP-8ADT induced similar mitochondrial  $Ca^{2+}$  overload (Figures 1K and S1P–S1R and Methods section).

Importantly, at the micromolar concentration (1  $\mu$ M) used in the present study, both TG and ASP-8ADT totally inhibit SERCA activity (Winther et al., 2010). Thus, differences observed in apoptosis induction were not correlated to differential action or affinity on SERCA activity. Moreover, in a previous study

(Dubois et al., 2013), we already observed that ASP-8ADT did not cause as much cell death during chronic exposure and we attributed this effect to a weaker ability of the ASP-8ADT compound to keep the ER stores depleted. However, this conclusion is ruled out in the present study, as we were unable to detect differences in the hallmarks of  $\text{Ca}^{2+}$  changes induced by TG or ASP-8ADT over a longer period covering the whole duration of apoptosis induction phase. We also checked that the uncoupling between  $\text{Ca}^{2+}$  homeostasis disruption and apoptosis induction did not result from impairments in ER stress response (Figures S1S–S1Y) or reactive oxygen species (ROS) accumulation in response to mitochondrial  $\text{Ca}^{2+}$  overload mediated by ASP-8ADT (Figure 1L). This in-depth study suggests the involvement of an undefined step/factor needed for an efficient cell death induction in response to  $\text{Ca}^{2+}$  homeostasis disruption and following mitochondrial  $\text{Ca}^{2+}$  overload.

### Mitochondrial $\text{Ca}^{2+}$ Overload Induces a Partial MPTP Opening, Ineffective to Induce Mitochondrial Membrane Depolarization and cyt c Release

It is generally considered that mitochondrial  $\text{Ca}^{2+}$  overload induces continuous MPTP openings during cell death, leading to loss of both  $\text{Ca}^{2+}$  and proton gradients across the inner mitochondrial membrane (Baumgartner et al., 2009; Giorgi et al., 2012). We used the gold standard calcein/ $\text{Co}^{2+}$ -quenching technique, which allows a quantification of MPTP opening (Bonora et al., 2016). We showed that an 18-h pretreatment with either TG (known to promote MPTP opening, Korge and Weiss, 1999) or ASP-8ADT was associated with a similar cobalt-mediated quenching of calcein fluorescence (Figures 2A and 2B) suggesting that MPTP was opened to an equivalent extent. This MPTP opening was abolished by a 1-h pretreatment with cyclosporine A (CsA; 0.5  $\mu\text{M}$ ), an inhibitor of MPTP opening that binds cyclophilin D. We also tested ionomycin (IM; 1  $\mu\text{M}$ ), a  $\text{Ca}^{2+}$  ionophore known to trigger mitochondrial  $\text{Ca}^{2+}$  overload and activation of MPTP in different cell models (Chaudhuri et al., 2016; Ying et al., 2018). We observed with IM a potent activation of MPTP compared with TG and ASP-8ADT (Figure 2C). In accordance, CsA pre-treatment (1 h before TG or ASP-8ADT treatments; 0.5  $\mu\text{M}$ ) induced an increase of mitochondrial  $\text{Ca}^{2+}$  content in response to TG or ASP-8ADT (Figure 2D). We concluded from these experiments that both ASP-8ADT and TG were able to induce similar but not maximal MPTP opening (as observed with IM). These experiments challenge the role of MPTP openings and mitochondrial  $\text{Ca}^{2+}$  overload implying that another process impaired cell death induction with ASP-8ADT. As a readout of cell death and MPTP openings, we evaluated the release of cyt c (Figures 2E, 2F, S2A, and S2B) and the loss of mitochondrial membrane potential (Figures 2G and 2H). Indeed, cyt c release from mitochondria and loss of mitochondrial membrane potential ( $\Delta\Psi_m$ ) are considered to occur subsequently to continuous pore activation. Our results clearly showed that ASP-8ADT failed to induce these features compared with TG and this despite its ability to induce both similar mitochondrial  $\text{Ca}^{2+}$  overload and MPTP opening. We also clearly demonstrated that TG induced only a partial mitochondrial depolarization when compared with the mitochondria uncoupler FCCP (1  $\mu\text{M}$ ) (Figures S2C and S2D). Our results also demonstrated that IM is a more potent inducer of MPTP opening than either ASP-8ADT or TG (Figure 2C). Thus, this partial MPTP opening induced by ASP-8ADT may explain that mitochondrial membrane potential is preserved with ASP-8ADT. Indeed, MPTP opening is intrinsically depolarizing, but we clearly showed that only partial MPTP opening occurs. Moreover, a situation with no mitochondrial  $\text{Ca}^{2+}$  overload occurred only when mitochondrial potential is totally collapsed by using FCCP as pretreatment (Figure 2D). Taken together, these results suggest that partial MPTP opening resulting from mitochondrial  $\text{Ca}^{2+}$  overload and ROS accumulation is not enough to induce loss of mitochondrial membrane potential and release of cyt c.

### Autophagy Inhibition Is a Prerequisite for Mitochondrial Depolarization Leading to Apoptosis Mediated by $\text{Ca}^{2+}$ Homeostasis Disruption

TG-treated cells exhibited mitochondrial membrane depolarization and efficient apoptosis induction, suggesting a direct link with its apoptotic potency. Interestingly, it has been reported that TG has significant implications in other  $\text{Ca}^{2+}$ -mediated and  $\text{Ca}^{2+}$ -independent signaling pathways such as autophagy (Bootman et al., 2018; Decuypere et al., 2011). We hypothesized that apoptosis mediated by TG could be related to the inhibition of survival pathways such as autophagy. We used, an established strategy, a tandem-tagged GFP-mCherry-LC3 probe that can determine whether an autophagosome has fused with a lysosome, based on the distinct chemical properties of GFP and mCherry fluorophores (Kimura et al., 2007). Under non-lysosomal and near-neutral pH conditions, both GFP and mCherry fluoresce. However, the low pH in the lumen of the lysosomes quenches the GFP signal, but not the mCherry. Using this approach, we found that upon TG treatment (2 h, 1  $\mu\text{M}$ ) in LNCaP cells, multiple autophagosomes are visible without GFP quenching, thereby suggesting that fusion with lysosomes did not occur (Figures 3A and 3B). In



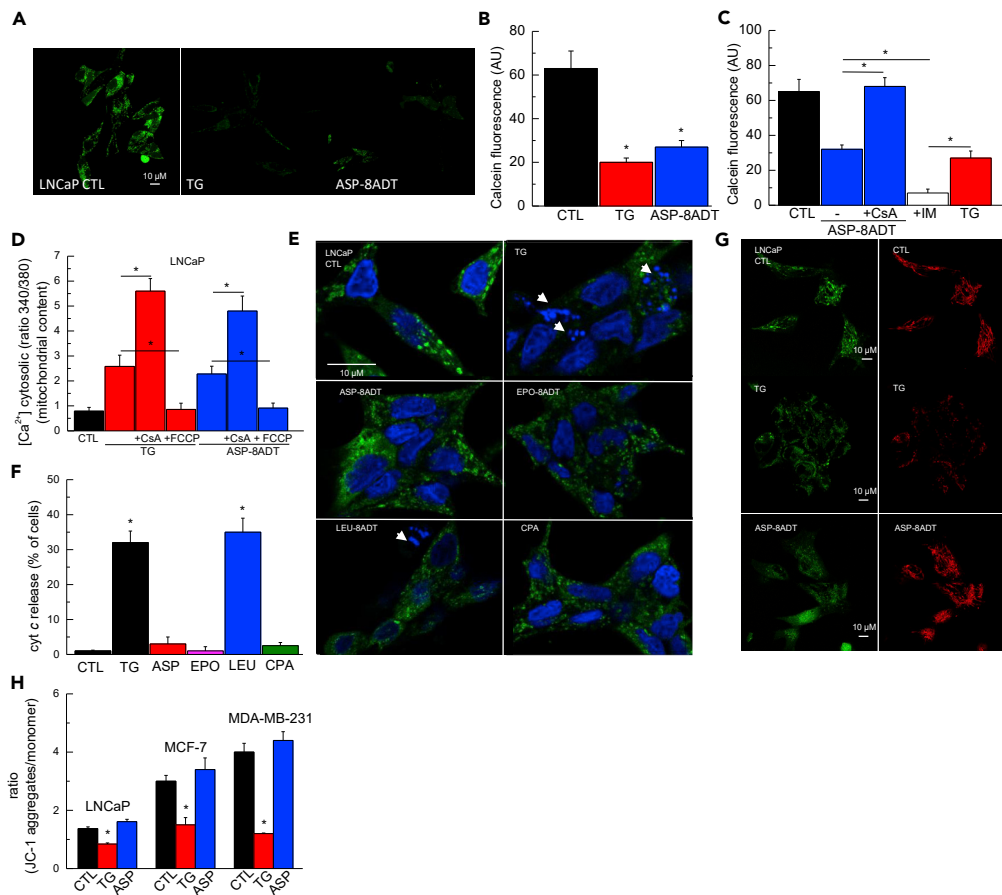


**Figure 2.  $\text{Ca}^{2+}$  Homeostasis Disruption and MPTP Opening**

(A) MPTP opening was assessed directly by the calcein/ $\text{Co}^{2+}$  method, and calcein fluorescence quenching was imaged 18 h after treatment with TG (1  $\mu\text{M}$ ) or ASP-8ADT (1  $\mu\text{M}$ ).

(B) Quantification of the results presented in (A).

(C) Effect of CsA and IM on MPTP opening assessed by calcein/ $\text{Co}^{2+}$  method 18 h after treatment with TG (1  $\mu\text{M}$ ) or ASP-8ADT (1  $\mu\text{M}$ ). (CsA, 0.5  $\mu\text{M}$ ; IM, 1  $\mu\text{M}$ ).

(D) Quantification of mitochondrial  $\text{Ca}^{2+}$  content in LNCaP cells subjected or not to cytosolic  $\text{Ca}^{2+}$  overload, 18 h after SERCA pump inhibition by TG or ASP-8ADT. CsA (0.5  $\mu\text{M}$ ) or FCCP (1  $\mu\text{M}$ ) pre-treatment (19 h; 1 h before SERCA pump inhibition).

(E) The subcellular distribution of cyt c 18 h after treatment in LNCaP cells, visualized using an anti-cyt c antibody (green fluorescence) using a confocal microscope. Arrows indicate apoptotic bodies or nuclei condensation (cell death) visualized by DAPI staining (blue). TG (1  $\mu\text{M}$ ), TG analogs (1  $\mu\text{M}$ ), and CPA (10  $\mu\text{M}$ ).

(F) Quantification of cyt c release (% of cells).

(G) Representative confocal images of LNCaP cells loaded with JC-1 dye 18 h after treatment with TG (1  $\mu\text{M}$ ) or ASP-8ADT (1  $\mu\text{M}$ ).

(H) Quantification of the fluorescence ratio (red fluorescence due to JC-1-aggregate/green fluorescence due to JC-1 monomers) from experiments presented in (G).

Experiments performed in triplicate. Bars represent mean  $\pm$  SEM. \* $p < 0.05$ , Student's t test.

contrast, upon ASP-8ADT treatment (2 h, 1  $\mu\text{M}$ ), only mCherry-positive structures have accumulated. The addition of chloroquine (CQ) (prevents endosomal acidification leading to an inhibition of lysosome-endosome fusion) in association with ASP-8ADT mimics the autophagic signature observed with TG. Indeed, by quantifying the size of acidic vesicles formed after treatment with TG, ASP-8ADT alone, or in combination with CQ, we observed an increase in size upon ASP-8ADT when combined with CQ to the same extent as TG (Figure 3C). In a second attempt, we evaluated the action of ASP-8ADT on the autophagic flux in LNCaP cells by using western blot analysis of LC3 I and II (formation of autophagosome) and P62 (autophagic flux) (Figures 3D–3F). These results confirmed previous studies that reported a block of autophagy by TG, as revealed by both accumulation of P62 and LC3 II. These effects were drastically reduced with ASP-8ADT,

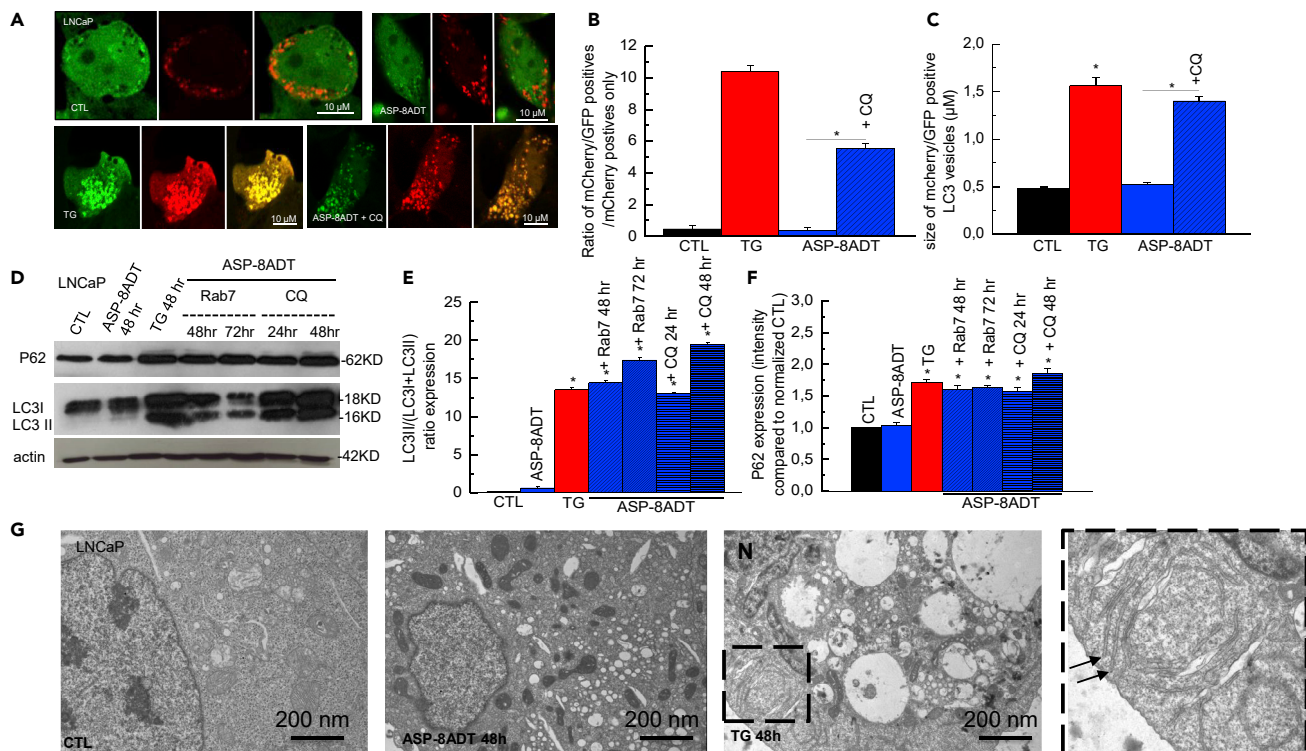


**Figure 3. Differential Effects of Thapsigargin Analogs on Autophagy**

(A) Representative confocal images of LNCaP cells transiently transfected with a tandem-tagged GFP-mCherry-LC3 probe and treated as indicated for 2 h with TG (1  $\mu$ M) or ASP-8ADT (1  $\mu$ M) alone or in combination with chloroquine (CQ, 25  $\mu$ M).  
 (B) Quantification of autophagic flux using the ratio (mCherry/GFP positives)/(mCherry positives only).  
 (C) Size of acid vesicles of the results presented in (A).  
 (D) Representative western blot of the autophagy marker protein P62 (upper panel) and LC3 I and II (middle panel) in LNCaP cells after treatment with control or the indicated drug with same concentration as used in (A). Rab7 inhibitory peptide (100 nM).  
 (E) Quantification of LC3 proteins using the ratio (LC3II)/(LC3I + LC3II) protein levels. Values represent the relative density of bands compared with the control condition, which will obviously have a relative density of 1. n = 3.  
 (F) Quantification of P62 protein levels. Values represent the relative density of bands compared with the control condition, which will obviously have a relative density of 1. n = 3.  
 (G) Electron microscopy images of LNCaP cells treated as indicated for 48 h with TG (1  $\mu$ M) or ASP-8ADT (1  $\mu$ M). The dashed line box is a magnification of a region of interest showing incomplete autophagic structures (unclosed autophagosome: black arrows).  
 Experiments performed in triplicate. Bars represent mean  $\pm$  SEM. \*p < 0.05, Student's t test.

thus revealing its inability to interfere with the autophagic process (Figures 3D–3F) (see also Figure S3). We also confirmed the action of ASP-8ADT and TG on autophagic flux in PC-3 prostate cancer cells and evaluated their action on autophagic flux in conditions of autophagy induction induced by starvation (Hanks' balanced salt solution [HBSS], 2 h) (Figures S3A–S3D). These results confirmed that TG is able to block autophagy, as revealed by both accumulation of P62 and LC3 II. These effects were greatly reduced with the ASP-8ADT compound. We also confirmed by real-time PCR of P62 mRNA levels that P62 protein level in ASP-8ADT-treated cells did not depend on variation of transcription (Figure S3D). We also checked the Beclin1 status (Figure S3E). We have further investigated the activity of TG on the autophagic process by using a more qualitative approach. By electron microscopy, we showed that only TG prevented the closure of the autophagosome and induced an accumulation of immature autophagosome that we never observed following ASP-8ADT treatment (Figure 3G).

We took advantage of the fact that ASP-8ADT did not exert an inhibitory effect on autophagy in LNCaP cells to study its implication on apoptosis induced by  $\text{Ca}^{2+}$  homeostasis disruption. We used a combined treatment with an ER  $\text{Ca}^{2+}$  stressor (TG or ASP-8ADT) and established autophagic inhibitors such as CQ, wortmannin (WT), bafilomycin A1 (Baf A1), and a Rab7 inhibitory peptide. Hoechst staining experiments showed, using autophagy inhibitors, a 6-fold increase of ASP-8ADT potency to induce cell death (from

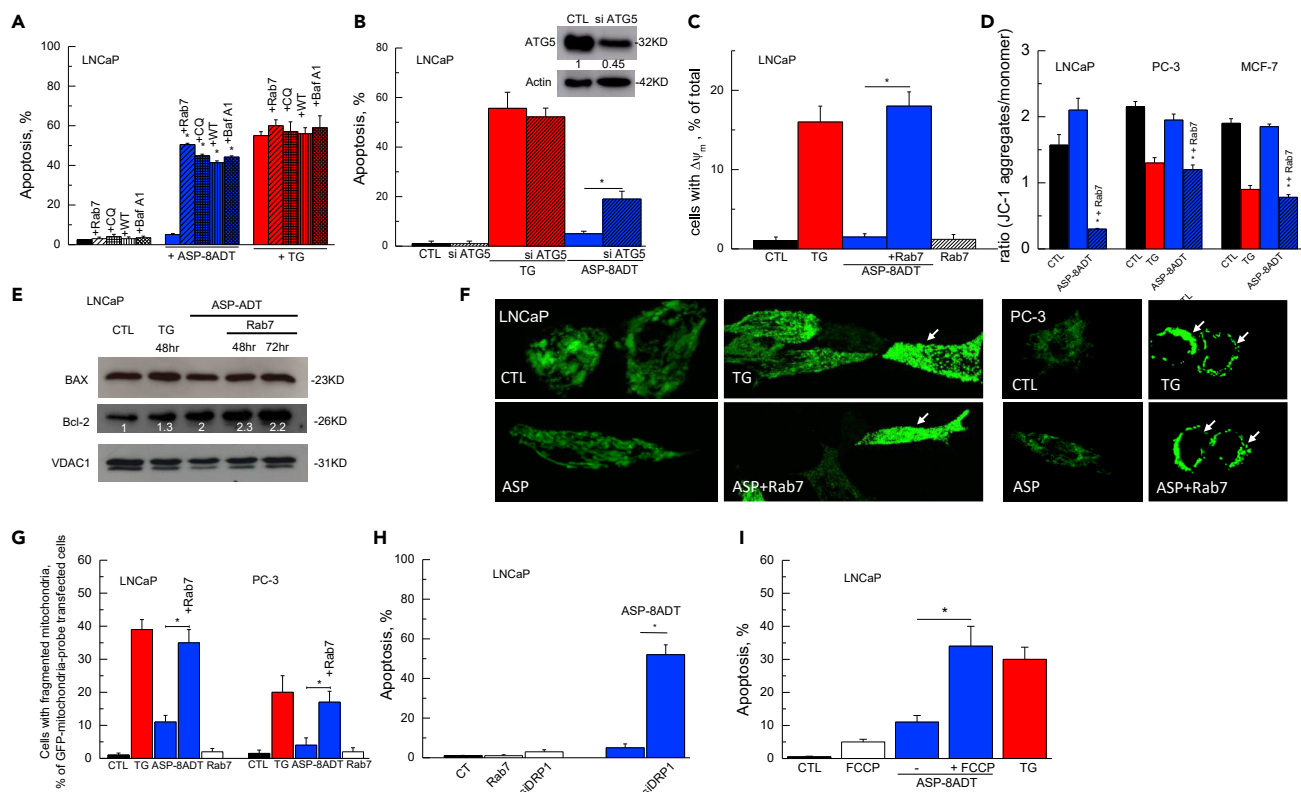


**Figure 4. Inhibition of Autophagy Determines the Pro-apoptotic Potential of Mitochondrial  $Ca^{2+}$  Overload Stimulus by Allowing Mitochondrial Fission and Membrane Depolarization**

(A and B) Quantification of apoptotic cells, as determined by manual counting of condensed nuclei following Hoechst staining, 48 h after treatment with control, ASP-8ADT alone, or in combination with autophagy inhibitors Rab7 inhibitory peptide (100 nM), chloroquine (CQ, 25  $\mu$ M), wortmannin (WT, 100 nM), and bafilomycin A1 (Baf A1, 100 nM). Cells were previously subjected to the indicated small interfering RNA (siRNA)-mediated silencing of ATG5 compared with control anti-luciferase siRNA (CTL) (24 h).

(C) Quantification of cells with depolarized mitochondria, as determined by the DiOC6(3) probe, 18 h after treatment with the indicated drug compared with CTL.

(D) Quantification of the fluorescence ratio from LNCaP, PC-3, and MCF-7 cells loaded with JC-1 dye 18 h after treatment.

(E) Representative western blot of the pro-apoptotic protein BAX and the anti-apoptotic protein Bcl-2 in LNCaP mitochondrial fraction after treatment.  $n = 3$ . (F) Representative confocal images of LNCaP and PC-3 cells transiently transfected with a GFP-mitochondria probe and treated as indicated for 18 h. White arrows indicate cells with mitochondrial fission.

(G) Quantification of cells with mitochondrial fission from the results presented in (F).

(H–I) Quantification of apoptotic cells, as determined by manual counting of condensed nuclei following Hoechst staining, 48 h after treatment with control or the indicated drug or with siRNA-mediated silencing of DRP-1 (24 h, 20 nM).  $n = 3$ . FCCP, 0.5  $\mu$ M. Experiments performed in triplicate. Bars represent mean  $\pm$  SEM. \* $p < 0.05$ , Student's t test.

5% to 30%), without additional effect on TG potency after 48 h treatment (Figure 4A). By western blot we confirmed the cleavage of PARP (Figure S4F) as a marker of caspase-dependent apoptosis. We also performed immunostaining of cyt c on LNCaP cells treated with ASP-8ADT (1  $\mu$ M, 18 h) alone or in combination with the autophagic inhibitor Rab7 (100 nM). Confocal images showed that ASP-8ADT induced the release of cyt c only upon autophagy inhibition (Figures S4A and S4B). We confirmed the requirement of autophagy inhibition with a genomic strategy by using small interfering RNA (siRNA) against ATG5, which participates in the formation of autophagosome (Ganley et al., 2011). Thereby, we showed that an early inhibition of the autophagic process by the down regulation of ATG5 leads to an increase in apoptosis induced by ASP-8ADT (Figure 4B). However, the percentage of apoptotic cells was not as high as with other inhibitors of autophagy (Figure 4A) or TG, because siRNA mediated knockdown of the autophagic regulatory gene ATG5 was only partial (Figure 4B, upper panel). By flow cytometry using the fluorescent mitochondrial membrane probe DiOC6(3), we demonstrated that Rab7 inhibitory peptide restored the ability of ASP-8ADT to induce mitochondrial membrane depolarization (Figure 4C). These results were confirmed using the JC-1 dye. We observed the progressive loss of red JC-1-aggregate fluorescence (polarized



mitochondria) and a cytoplasmic diffusion of green monomer fluorescence (depolarized mitochondria) following exposure to ASP-8ADT in combination with Rab7 inhibitor (Figure 4D). We confirmed this specific point in prostate LNCaP, PC-3, and breast MCF-7 cancer cell lines (Figure 4D). Thus, these data clearly demonstrated that inhibition of autophagy is required for efficient mitochondrial membrane depolarization upon mitochondrial  $\text{Ca}^{2+}$  overload leading to the release of cyt c and apoptosis induction. Finally, we investigated the potential role of BAX and BCL-2 proteins, two crucial actors involved in the mitochondrial apoptotic pathway, by studying their expression and subcellular distribution at mitochondria in LNCaP cells. Using subcellular fractionation technique, we observed that BAX level was nearly the same at mitochondria following treatments with TG or ASP-8ADT alone or in combination with autophagy inhibition. In contrast, BCL-2 expression was higher in all the conditions compared with control (Figure 4E). These findings suggest that OMM permeabilization driven by BAX and BCL-2 interactions is not a critical event in apoptosis induced by TG or ASP-8ADT (in combination with autophagy inhibition). Thus the weaker ability of ASP-8ADT to kill the cells could not be explained by the promotion of the BCL-2 survival pathway.

### **Concomitant Inhibition of Autophagy and Mitochondrial $\text{Ca}^{2+}$ Overload Is Required for Inducing an Acute Mitochondrial Stress Revealed by a DRP1-Mediated Mitochondrial Dynamic Remodeling**

We further explored the consequences of mitochondrial  $\text{Ca}^{2+}$  overload and autophagy inhibition in the control of cell fate. It is well known that mitochondrial dynamics (fusion and fission) and autophagy work together as a quality control mechanism in the life cycle of the mitochondrion (Twig et al., 2008). During the apoptotic process, mitochondrial networks are dramatically reorganized from long filamentous interconnected tubules into small punctate spheres. Whether remodeling of mitochondrial networks is necessary for apoptosis-associated cyt c release, or is merely an accompanying process, is still a subject of debate (Sheridan and Martin, 2010). 3D reconstruction from confocal imaging experiments clearly showed that the filamentous interconnected tubules of the mitochondrial networks were preserved with ASP-8ADT alone but disrupted when combined with autophagy inhibitor as observed with TG (Figures 4F and 4G). These results clearly showed that mitochondrial  $\text{Ca}^{2+}$  overload alone did not induce significant changes in mitochondrial dynamics suggesting that cell fate was not compromised when autophagy can play its pro-survival role. On the contrary, concomitant inhibition of autophagy forced the cell to use another pro-survival pathway mediated by mitochondrial dynamics. Indeed, recent studies have demonstrated that under sustained stress conditions, a DRP1-dependent mitochondrial fission is triggered and is involved in cellular survival at the early stage of injury (Ikeda et al., 2014; Zuo et al., 2014). In this context, we showed that siRNA-mediated knockdown of DRP1 restored the apoptotic potential of ASP-8ADT (Figure 4H) confirming the crucial role of mitochondrial dynamics. siDRP1 treatments were functionally validated by confocal microscopy using MitoTracker Red CMXRos staining (via the observation of the characteristic mitochondrial hyperfusion) and western blot (Figures S4C–S4E). These results showed that a mitochondrial dynamic remodeling mediated by DRP1 is triggered and is involved in cell survival only when cells were exposed to concomitant  $\text{Ca}^{2+}$  homeostasis disruption and autophagy inhibition. However, this pro-survival mechanism is not sufficient to prevent apoptosis induction induced by TG or ASP-8ADT in combination with autophagic inhibitors. These results also pointed out that autophagy and fission/fusion mitochondrial dynamics are two processes that could be used by the cell to counteract the mitochondrial stress mediated by  $\text{Ca}^{2+}$  overload. These pro-survival pathways prevent mitochondrial collapse by inhibiting mitochondrial membrane depolarization. In fact, mitochondrial membrane depolarization seems to be the last and decisive event preceding apoptosis in response to mitochondrial  $\text{Ca}^{2+}$  overload. We confirmed this feature by using FCCP (0.5  $\mu\text{M}$ , 48 h) to induce mitochondrial membrane depolarization, and indeed, FCCP restored the ability of ASP-8ADT to induce cell death, whereas used alone it failed to do this significantly (Figure 4I).

### **Dual Targeting of $\text{Ca}^{2+}$ Homeostasis and Autophagy Improves Chemotherapy Efficiency In Vitro and In Vivo**

Targeting mitochondria or autophagy to sensitize cancer cells to apoptosis is a major aim in anti-cancer therapy (Jiang et al., 2015; Kroemer, 2015; Wen et al., 2013; White, 2015; Zhang et al., 2016), and the medical and scientific community has also come to accept that monotherapy is unlikely to be the answer to completely destroy cancer cells (Hanahan, 2014). Our results confirm that targeting mitochondrial  $\text{Ca}^{2+}$  homeostasis alone displays only poor efficiency. The molecular basis underlying this lack of efficiency is that apoptosis mediated by mitochondrial  $\text{Ca}^{2+}$  overload requires inhibition of autophagy. This new interplay

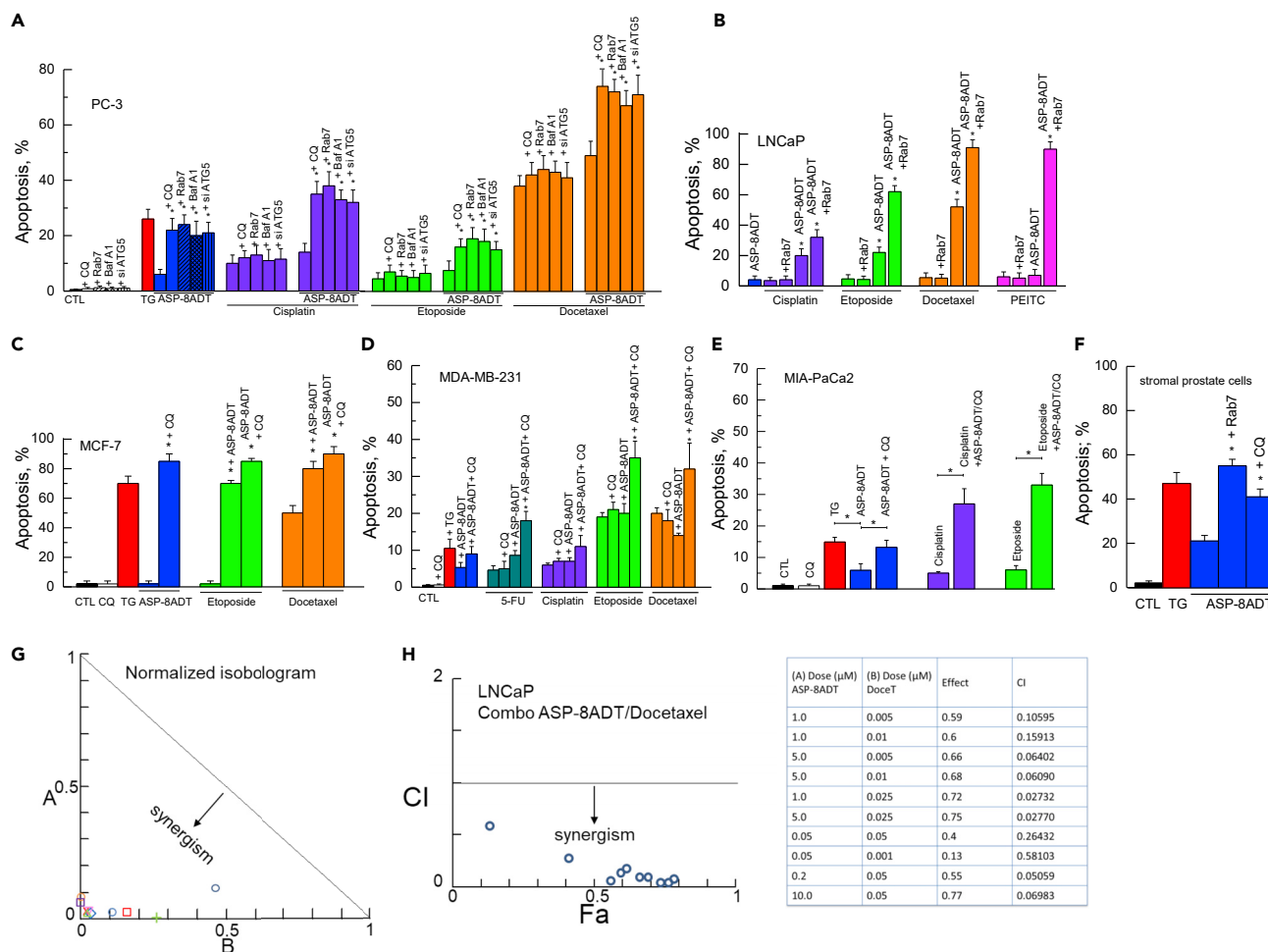


**Figure 5. A Co-targeting Strategy Based on Mitochondrial  $\text{Ca}^{2+}$  Overload and Autophagy Inhibition Represents a Crucial Determinant of Chemosensitivity**

(A–F) Quantification of apoptotic cells, as determined by Hoechst staining, 48 h after ASP-8ADT or TG treatment with control or the indicated drugs in PC-3 cells (A), LNCaP (B), MCF-7 (C), MDA-MB-231 (D), MIA-PaCa2 (E), and stromal prostate cancer cells (F).  $n = 3$ .

(G and H) Isobologram and combination index (CI) analyses for evaluating ASP-8ADT/docetaxel interactions in combination in LNCaP cells. Dose effect response curves were performed in the background of autophagy inhibition by the use of CQ, and isobologram analyses were performed. Experiments performed in triplicate. Bars represent mean  $\pm$  SEM. \* $p < 0.05$ , Student's *t* test.

challenges a crucial paradigm in cell death, and our results reveal novel combinatorial therapeutic strategies to improve clinical outcomes.

ASP-8ADT is the active compound of the mipsagargin family, a promising new anti-cancer treatment approved by the US Food and Drug Administration (FDA) and used in several clinical trials (NCT01056029 and NCT01734681) (Denmeade and Isaacs, 2005; Mahalingam et al., 2016). Unfortunately, results are below expectations as published in a recent report (Mahalingam et al., 2016). Based on our fundamental findings we have evaluated using xenograft mouse models, cell line-based functional studies, and *ex vivo* tumor models from clinical specimens, the relevance of our combined strategy to (1) increase the efficiency of ASP-8ADT *in vivo* and (2) sensitize cancer cells to chemotherapies using a co-targeting strategy. Cancer-specific conventional chemotherapeutic agents have been used in combination with ER stressor agents and autophagy inhibition for six models of cancer: PC-3 (Figure 5A) and LNCaP (Figure 5B), primary human stromal prostate cancer cells (Figure 5F), MCF-7 and MDA-MB-231 breast cancer cells (Figures 5C and 5D), and MIA-PaCa2 pancreatic cancer cells (Figure 5E). Interestingly, in almost all conditions, the different autophagic inhibitors failed to significantly increase the chemotherapeutic apoptotic index. In contrast, ASP-8ADT used in combination with an autophagic inhibitor frequently increased

chemotherapeutic cytotoxicity, regardless of the action mechanism, thus suggesting a unique way of priming cancer cells for several conventional cancer therapies. In the case of stromal prostate cancer cells and mammary cancer cells MCF-7, ASP-8ADT with autophagy inhibition induced high levels of apoptosis even in the absence of chemotherapy (Figures 5C and 5F). Most of our combined therapies were due to a synergic effect of the treatment (example of the analysis can be found in Figures 5G, 5H, and S5A–S5C). Only few conditions were simply additive effects (pancreatic cell lines for cisplatin and 5-fluorouracil [5-FU], cisplatin, docetaxel on MDA-MB-231).

We also conducted a series of combined therapy experiments on nude mice using prostate and breast tumor xenografts. The proof of principle concerning G-202 is well established *in vivo* (Denmeade et al., 2012), and in clinical trials, G-202 is injected intravenously. However, G-202 efficiency is also associated with an anti-angiogenic effect that may bias our results when used in *in vivo* experiments with chemotherapeutic agents such as taxotere (docetaxel). Thus, in our experiments, to achieve ER  $\text{Ca}^{2+}$  stress, tumors were injected intratumorally (i.t.) at the rate of six injections over 2 weeks with ASP-8ADT alone (1  $\mu\text{M}$ /PBS) or in combination with CQ (50  $\mu\text{M}$ /PBS). The results of these experiments revealed that animals treated with a combined therapy displayed significantly less tumor growth than animals treated with ASP-8ADT alone (Figure 6A) associated with increased cell death, as revealed by TUNEL staining (Figure 6B) and PARP cleavage (Figure 6C). We also assessed the ability of the combined therapy in priming cancer cells to a classical chemotherapeutic agent such as docetaxel or 5-FU on, respectively, prostate and breast xenografts. To reduce the number of mice used, accordingly to our strict ethical rules, we have focused our experiment on proving the efficiency of the combined therapy and consequently did not assess docetaxel or 5-FU alone (based on the literature and strong *in vitro* data). The combined therapy (ASP-8ADT/CQ) again significantly increased the capacity of docetaxel and 5-FU to reduce tumor growth and increase apoptosis index when compared with docetaxel or 5-FU and CQ alone (Figures 6D–6H). Concerning breast xenografts, the inhibition of tumor growth in mice treated with a combined therapy is correlated with a drastic increase in the proportion of cells that underwent apoptosis, as revealed by TUNEL staining (Figure S6). We have used fresh human tumor samples from prostate in an *ex vivo* slices tumor assay to confirm the efficiency of autophagy inhibition on ASP-8ADT anti-tumor activity alone or combined with conventional chemotherapy. This *ex vivo* tumor assay is an excellent tool as it keeps tumor heterogeneity and allows the clinical response to anti-cancer drugs to be predicted (Majumder et al., 2015). In these experiments, human prostate tumors were treated with a complete panel of treatments. First, we confirmed the efficiency of autophagy inhibition on ASP-8ADT anti-tumor activity with an important increase in the proportion of cells undergoing apoptosis, as revealed by TUNEL staining (Figure 6I). Second, the combined therapy (ASP-8ADT/CQ) significantly increased the capacity of docetaxel/CQ to induce apoptosis (Figure 6I). Altogether, these assays clearly showed that inhibition of autophagy rescues the anti-cancer activity of ASP-8ADT and that a combined therapy based on a  $\text{Ca}^{2+}$  stress and inhibition of autophagy increases chemosensitivity to docetaxel and 5-FU of prostate and breast cancers, respectively.

## DISCUSSION

In a previous work, we uncovered an atypical mode to escape from cell death in response to  $\text{Ca}^{2+}$  homeostasis perturbations (Dubois et al., 2016, 2013), but the precise molecular mechanisms were not investigated. Here we identified autophagy and mitochondrial fission as gatekeepers in the paradigm referred as the  $\text{Ca}^{2+}$  apoptosis link (Berridge et al., 2000). This dependency has never been identified before as a required step. Our most important finding is also that  $\text{Ca}^{2+}$ -induced MPTP opening cannot be longer considered as a potent apoptosis activator just by itself. Indeed, one of our most striking results is that whereas TG and its analog ASP-8ADT induce similar ER, cytosolic, and mitochondrial  $\text{Ca}^{2+}$  dynamics leading to MPTP opening, apoptosis induced by ASP-8ADT is very modest (Figures 1 and 2). We show that this “loss of function” is linked to its inability to block autophagy as it has been described for TG (Engedal et al., 2013; Ganley et al., 2011; Sætre et al., 2015), thereby revealing a direct and crucial role of autophagy in the  $\text{Ca}^{2+}$  apoptosis link (Figure 3). This feature may be supported by the fact that TG and ASP-8ADT have similar but not identical chemical structure (Dubois et al., 2013). Originally it has been suggested that the inhibitory effect of TG on the autophagic flux was independent of a functional ER stress response, but could be related to the activity of TG to inhibit SERCA and thus to influence downstream  $\text{Ca}^{2+}$  signaling pathways involved in the regulation of autophagy (Ganley et al., 2011). Our results are not in accordance with this possibility because ASP-8ADT induces both similar ER stress response and remodeling of  $\text{Ca}^{2+}$  homeostasis as TG (Figure 1). This implies that TG targets an unidentified molecular mechanism

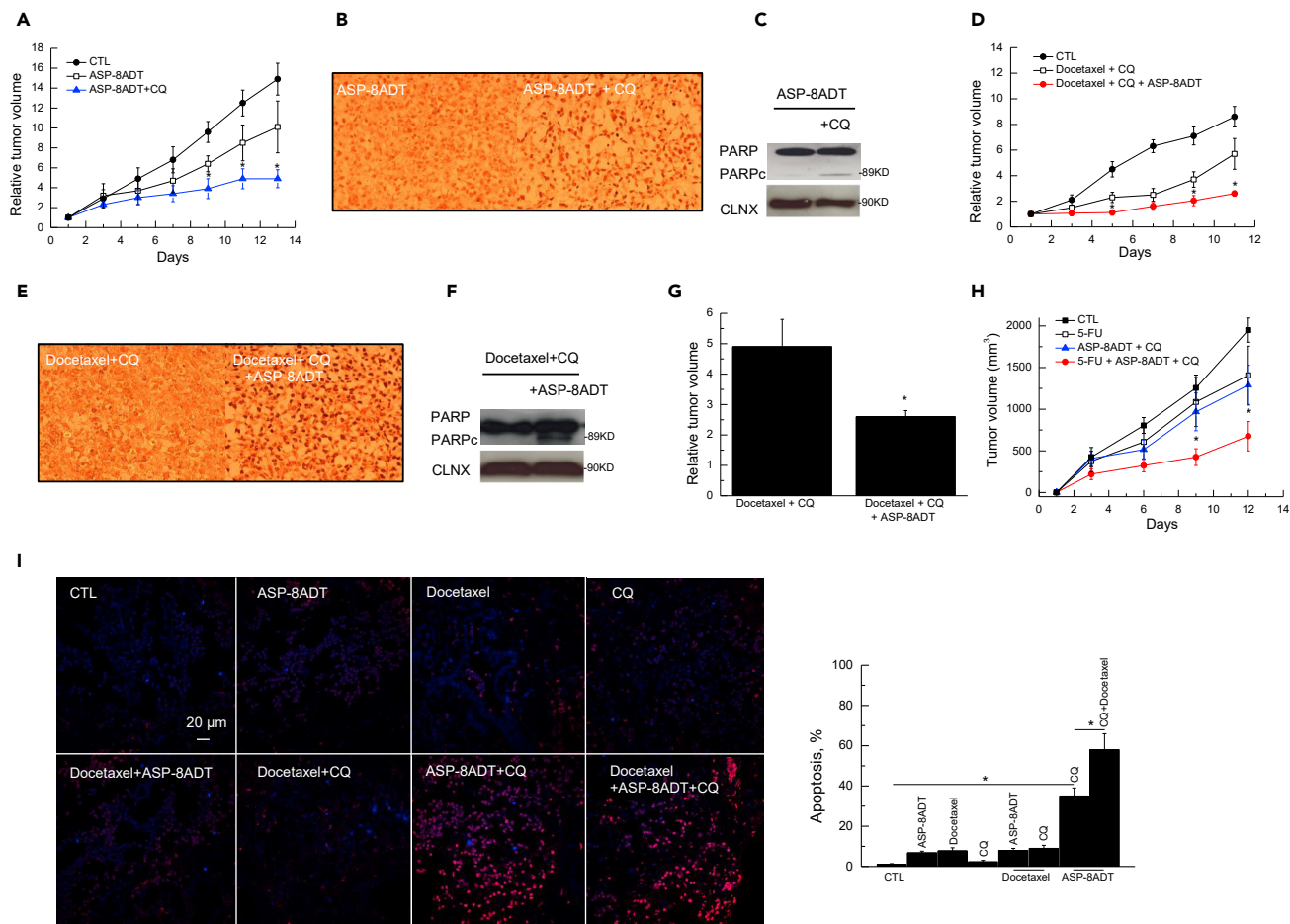


**Figure 6. Priming Cancer Cells by a Concomitant Inhibition of Autophagy and Ca<sup>2+</sup> Stress Stimulation in Mouse Xenograft Tumor Assays and in Primary Human Tumor Explants**

(A) The relative volume of PC-3 cell xenograft tumors over time in nude mice treated for 2 weeks with ASP-8ADT alone or in combination with CQ.  
 (B) TUNEL staining obtained from tumor treated in (A). Colorimetric TUNEL apoptosis assay is used for detection of apoptosis. The 3'-OH end of the DNA strand breaks in apoptotic cells is labeled with biotinylated nucleotides using the enzyme TdT. Streptavidin-conjugated horseradish peroxidase (HRP) is then bound to the biotinylated nucleotides and visualized using the peroxidase substrate, 3,3'-diaminobenzidine (DAB). The nuclei of apoptotic cells should be observed dark brown under light microscope.  
 (C) A representative western blot of the apoptosis marker protein PARP from tumors treated in (A).  
 (D) The relative volume of PC-3 cell xenograft tumors over time in nude mice treated for 2 weeks with docetaxel (10 mg/kg) alone or in combination with ASP-8ADT/CQ.  
 (E) TUNEL staining obtained from tumor slices treated in (D).  
 (F) A representative western blot of the apoptosis marker protein PARP from tumors treated in (E).  
 (G) Quantification of the relative tumor volume of PC-3 cell xenograft tumors treated for 2 weeks with docetaxel/CQ or docetaxel/CQ/ASP-8ADT.  
 (H) The volume of MDA-MB-231 cell xenograft tumors over time in nude mice treated for 2 weeks with the indicated drugs. N = 3 and n = 5 per condition for (A), (D), and (H).  
 (I) Representative images of human prostate tumor sections labeled with Hoechst and TUNEL for apoptosis detection after *ex vivo* treatments with the indicated drugs (48 h). n = 4. Bars represent mean  $\pm$  SEM. \*p < 0.05, Student's t test. The significance of the differences was analyzed using Student's t test at the end of the *in vivo* experiments.

preferentially implicated in the closure of autophagosomes as it has been suggested in a previous study (Engedal et al., 2013). Nonetheless, we were able to restore the pro-apoptotic potency of ASP-8ADT by using pharmacological or genetic inhibition of autophagy.

We also demonstrated that both TG and ASP-8ADT induced potent mitochondrial Ca<sup>2+</sup> overload that causes MPTP opening. However, we observed that mitochondria are still able to retain large amounts of Ca<sup>2+</sup> and surprisingly, that the mitochondrial membrane potential could be preserved. These findings

seem to be in contradiction with the fact that when MPTP is open, both  $\text{Ca}^{2+}$  and proton gradients across the inner mitochondrial membrane are dissipated. In fact, we identified that a situation with totally depleted mitochondria from  $\text{Ca}^{2+}$  can occur only when mitochondrial potential is totally collapsed by using a protonophore such as FCCP (Figure 4). Indeed, we observed that TG induced only partial mitochondrial depolarization compared with FCCP, and we suggest that this feature could explain the retention of  $\text{Ca}^{2+}$ . In fact, our results are in accordance with some studies in that the process of MPTP opening at the cellular level does not obey all-or-none law as it has been suggested in other models (Dumas et al., 2009). Concerning ASP-8ADT, the mitochondrial membrane potential was virtually not affected despite the opening of MPTP, suggesting that other mechanisms can potentially play a crucial role for maintaining mitochondrial membrane potential. In particular, we identified autophagy and mitochondrial dynamics as two crucial steps involved in the maintenance of mitochondrial potential (Figures 3 and 4). Interestingly, we demonstrated that the pro-survival action of autophagy or mitochondrial dynamics could be used sequentially by the cells to try to overcome the stress mediated by mitochondrial  $\text{Ca}^{2+}$  overload (Figure 4). Indeed, in the case of autophagy impairment, cells switch from the pro-survival autophagy pathway to a DRP-1-mediated mitochondrial dynamics to try to overcome the stress mediated by mitochondrial  $\text{Ca}^{2+}$  overload, highlighting the role of DRP1 for maintaining mitochondrial potential as observed in other study (Choi et al., 2013). In this context, our results clearly indicated that the pharmacological or genetic impairment of DRP-1 could be used to restore the  $\text{Ca}^{2+}$ -apoptosis link.

Thus, our study highlights the central role of autophagy and mitochondrial dynamics as survival mechanisms ensuring the integrity of mitochondrial membrane potential during mitochondrial  $\text{Ca}^{2+}$  overload stress. For this reason, the targeting of autophagy or mitochondrial dynamics could be used to promote apoptosis in cancer cells subjected to mitochondrial  $\text{Ca}^{2+}$  overload.

Our preclinical data confirmed that the use of CQ or Rab7 GTPase inhibitor by inhibiting autophagy increases chemotherapy efficiency in several cancer models *in vitro*. As a proof of concept, we confirmed the potential translational significance of our combined strategy with conventional drugs used in clinic or in clinical evaluation (i.e., ASP-8ADT). For this, we used both classical *in vivo* approach (xenograft mouse model) and an *ex vivo* strategy with human clinical specimens of prostate and breast cancer (Figure 6 and S6). This *ex vivo* strategy allows the prediction of the clinical response to anti-cancer drugs by maintaining tumor heterogeneity (Majumder et al., 2015). In the case of prostate cancer treatment, we have used docetaxel, which was the first chemotherapeutic agent to increase survival time in patients with androgen-resistant prostate cancer. For breast cancer we have evaluated the conventional treatment 5-FU. The ASP-8ADT compound used in our study to induce sustained mitochondrial perturbations corresponds to the active ingredient of the mipsagargin pro-drug (G-202) (Denmeade et al., 2012) currently under evaluation as potential targeted therapy for prostate cancer, gliomas, clear cell renal cancer, or hepatocarcinomas. In a clinical study on patients with advanced solid tumors receiving mipsagargin, the authors did not observe a clinical response, but a prolonged disease stabilization was observed in a subset of patients (Mahalingam et al., 2016). In this context, our findings may benefit patients by improving the clinical outcome associated with G-202 treatment. Indeed, our fundamental findings redefine the molecular pathways underlying the anti-tumor activity of ASP-8ADT (G-202) as we clearly demonstrated that concomitant inhibition of autophagy is required. In agreement with these findings, we proposed two new combined anti-cancer therapies (1) G-202 combined with CQ and (2) G-202 combined with CQ and a standard chemotherapy. Concerning the combination with a standard chemotherapy, we clearly demonstrated that the combination of ASP-8ADT and docetaxel in the background of autophagy inhibition showed synergistic interactions (Figure 6). It is also well known that mitochondrial priming mediated by BCL-2 family proteins correlates with clinical response to cytotoxic chemotherapy (Ni Chonghaile et al., 2011). Indeed, permeabilization of the OMM is considered to be the decisive event in the onset of cell death (Kroemer et al., 2007) and is subject to a tight control by pro- and anti-apoptotic members of the BCL-2 protein family (Czabotar et al., 2014). Interestingly, the mechanism identified here for the sensitivity and the resistance to cancer therapies seems to be a BCL-2-independent mechanism, and thus, it may represent an innovative therapeutic approach. Importantly, all the compounds used in our proposed combination therapies have been approved by the FDA. All compounds used in our combined therapies have also distinct mechanisms of anti-tumor activity, ruling out a possible competitive impairment, and both CQ and G-202 have already demonstrated an acceptable tolerability (Manic et al., 2014). Such combined therapy using a targeted anti-cancer agent such as mipsagargin in combination with a standard chemotherapy and inhibition of autophagy is a realistic approach. Recently, Inspyr Therapeutics (G-202) has initiated a pre-clinical study



evaluating the potential of G-202 in combination with Nexavar, using liver tumor models that express prostate-specific membrane antigen, the target of G-202. Moreover, numerous clinical studies also evaluate combined therapies including two, three, or four compounds. In particular, the combination of oxaliplatin, irinotecan, and 5-FU (FOLFOXIRI) in association with bevacizumab demonstrated in a phase III trial to improve outcome and became a new standard regimen for initial therapy of metastatic colorectal cancer (Loupakis et al., 2014).

In conclusion, these findings challenge a crucial paradigm in cell death revealing a novel and promising priming strategy to improve clinical outcomes for patients with solid cancers.

### Limitations of the Study

Based on the results derived from pharmacological induction of mitochondrial  $\text{Ca}^{2+}$  overload in cultured cells and xenograft mouse models, we were able to demonstrate that, by inhibiting the autophagy pathway, mitochondrial  $\text{Ca}^{2+}$  status can modulate chemosensitivity. However, the conclusions would be strengthened if the precise molecular mechanism underlying autophagy inhibition and mediated by TG was identified. Moreover, the physiological and pathophysiological aspects of this new interplay between  $\text{Ca}^{2+}$  signaling and autophagy in the regulation of mitochondrial cell fate should be confirmed in the context of pathologies associated with mitochondrial disorders (neurodegenerative and cardiovascular diseases, diabetes, or myopathies).

### Resource Availability

#### Lead Contact

[fabien.vanden-abeele@inserm.fr](mailto:fabien.vanden-abeele@inserm.fr).

#### Materials Availability

Further information required to interpret, replicate, or build upon the methods or findings reported in the article is available from the corresponding author upon request ([Fabien.vanden-abeele@inserm.fr](mailto:Fabien.vanden-abeele@inserm.fr)).

#### Data and Code Availability

There is no dataset and/or code associated with the article.

## METHODS

All methods can be found in the accompanying [Transparent Methods supplemental file](#).

## SUPPLEMENTAL INFORMATION

Supplemental Information can be found online at <https://doi.org/10.1016/j.isci.2020.101263>.

## ETHICS DECLARATIONS

The present study was approved by Ethics Committee of GHICL Hospital, Hospital St-Philibert, Lomme, France.

Studies involving animals, including housing and care, method of euthanasia, and experimental protocols, were conducted in accordance with the local animal ethical committee in the animal house (C59-00913; protocol CEEA 202012) of the University of Sciences and Technologies of Lille, under the supervision of Dr. Lehen'kyi (59-009270).

## ACKNOWLEDGMENTS

We acknowledge Prof R. Tsien for generously providing 4mtTM3cpv Cameleon construct and Prof J. Vuust Møller & Prof B. Christensen for providing thapsigargin analogs. Graphical Abstract was adapted from Servier Medical Art, licensed under a Creative Common Attribution 3.0 Generic License. <http://smart.servier.com/>.

This work was supported by a grant from Comité Septentrion de la Ligue contre le cancer to F.V.A. and La Fondation de France to C.D.

## AUTHORS CONTRIBUTIONS

C.D. designed research studies, performed most of the experiments, conceived the experimental designs, analyzed the data, and drafted the manuscript. A.K., L.N., and G.B. performed experiments and analyzed the data. E.V., F.V.A., and R.-A.T. performed experiments. M.R. provided primary human stromal prostate cancer cells. D.T. participated in *in vivo* and *ex vivo* experiments. J.-L.B. provided primary human prostate cancer cells. N.P. provided advice. F.V.A. directed the study, designed research studies, performed the experiments, conceived the experimental designs, analyzed the data, and drafted the manuscript.

## DECLARATION OF INTERESTS

The authors declare that they have no competing interests.

Received: March 16, 2020

Revised: April 17, 2020

Accepted: June 8, 2020

Published: July 24, 2020

## REFERENCES

- Baumgartner, H.K., Gerasimenko, J.V., Thorne, C., Ferdek, P., Pozzan, T., Tepikin, A.V., Petersen, O.H., Sutton, R., Watson, A.J.M., and Gerasimenko, O.V. (2009). Calcium elevation in mitochondria is the main Ca<sup>2+</sup> requirement for mitochondrial permeability transition pore (mPTP) opening. *J. Biol. Chem.* **284**, 20796–20803.
- Berridge, M.J., Bootman, M.D., and Roderick, H.L. (2003). Calcium signalling: dynamics, homeostasis and remodelling. *Nat. Rev. Mol. Cell Biol.* **4**, 517–529.
- Berridge, M.J., Lipp, P., and Bootman, M.D. (2000). The versatility and universality of calcium signalling. *Nat. Rev. Mol. Cell Biol.* **1**, 11–21.
- Bonora, M., Morganti, C., Morciano, G., Giorgi, C., Wieckowski, M.R., and Pinton, P. (2016). Comprehensive analysis of mitochondrial permeability transition pore activity in living cells using fluorescence-imaging-based techniques. *Nat. Protoc.* **11**, 1067–1080.
- Bootman, M.D., Chehab, T., Bultynck, G., Parys, J.B., and Rietdorf, K. (2018). The regulation of autophagy by calcium signals: do we have a consensus? *Cell Calcium* **70**, 32–46.
- Chaudhuri, D., Artiga, D.J., Abiria, S.A., and Clapham, D.E. (2016). Mitochondrial calcium uniporter regulator 1 (MCUR1) regulates the calcium threshold for the mitochondrial permeability transition. *Proc. Natl. Acad. Sci. U S A* **113**, E1872–E1880.
- Chen, Y., and Klionsky, D.J. (2011). The regulation of autophagy - unanswered questions. *J. Cell Sci.* **124**, 161–170.
- Choi, S.Y., Kim, J.Y., Kim, H.-W., Cho, B., Cho, H.M., Oppenheim, R.W., Kim, H., Rhyu, I.J., and Sun, W. (2013). Drp1-mediated mitochondrial dynamics and survival of developing chick motoneurons during the period of normal programmed cell death. *FASEB J.* **27**, 51–62.
- Clapham, D.E. (2007). Calcium signaling. *Cell* **131**, 1047–1058.
- Czabotar, P.E., Lessene, G., Strasser, A., and Adams, J.M. (2014). Control of apoptosis by the BCL-2 protein family: implications for physiology and therapy. *Nat. Rev. Mol. Cell Biol.* **15**, 49–63.
- Decuypere, J.-P., Bultynck, G., and Parys, J.B. (2011). A dual role for Ca<sup>2+</sup> in autophagy regulation. *Cell Calcium* **50**, 242–250, Special issue on Ca<sup>2+</sup> signaling mechanisms of cell survival and cell death.
- Degenhardt, K., Mathew, R., Beaudoin, B., Bray, K., Anderson, D., Chen, G., Mukherjee, C., Shi, Y., Gélinas, C., Fan, Y., et al. (2006). Autophagy promotes tumor cell survival and restricts tumor necrosis, inflammation, and tumorigenesis. *Cancer Cell* **10**, 51–64.
- Denmeade, S.R., and Isaacs, J.T. (2005). The SERCA pump as a therapeutic target: making a “smart bomb” for prostate cancer. *Cancer Biol. Ther.* **4**, 14–22.
- Denmeade, S.R., Mhaka, A.M., Rosen, D.M., Brennen, W.N., Dalrymple, S., Dach, I., Olesen, C., Gurel, B., Demarzo, A.M., Wilding, G., et al. (2012). Engineering a prostate-specific membrane antigen-activated tumor endothelial cell prodrug for cancer therapy. *Sci. Transl. Med.* **4**, 140ra86.
- Dubois, C., Prevarskaya, N., and Vanden Abeele, F. (2016). The calcium-signaling toolkit: Updates needed. *Biochim. Biophys. Acta* **1863**, 1337–1343.
- Dubois, C., Vanden Abeele, F., Sehgal, P., Olesen, C., Junker, S., Christensen, S.B., Prevarskaya, N., and Møller, J.V. (2013). Differential effects of thapsigargin analogues on apoptosis of prostate cancer cells: complex regulation by intracellular calcium. *FEBS J.* **280**, 5430–5440.
- Dumas, J.F., Argaud, L., Cottet-Rousselle, C., Vial, G., Gonzalez, C., Detaille, D., Leverve, X., and Fontaine, E. (2009). Effect of transient and permanent permeability transition pore opening on NAD(P)H localization in intact cells. *J. Biol. Chem.* **284**, 15117–15125.
- Engedal, N., Torgersen, M.L., Guldvik, I.J., Barfeld, S.J., Bakula, D., Sætre, F., Hagen, L.K., Patterson, J.B., Proikas-Cezanne, T., Seglen, P.O., et al. (2013). Modulation of intracellular calcium homeostasis blocks autophagosome formation. *Autophagy* **9**, 1475–1490.
- Ganley, I.G., Wong, P.-M., Gammoh, N., and Jiang, X. (2011). Distinct autophagosomal-lysosomal fusion mechanism revealed by thapsigargin-induced autophagy arrest. *Mol. Cell* **42**, 731–743.
- Giorgi, C., Baldassari, F., Bononi, A., Bonora, M., De Marchi, E., Marchi, S., Missiroli, S., Patergnani, S., Rimessi, A., Suski, J.M., et al. (2012). Mitochondrial Ca(2+) and apoptosis. *Cell Calcium* **52**, 36–43.
- Giorgi, C., Ito, K., Lin, H.-K., Santangelo, C., Wieckowski, M.R., Lebedzinska, M., Bononi, A., Bonora, M., Duszynski, J., Bernardi, R., et al. (2010). PML regulates apoptosis at endoplasmic reticulum by modulating calcium release. *Science* **330**, 1247–1251.
- Hanahan, D. (2014). Rethinking the war on cancer. *Lancet* **383**, 558–563.
- Hanahan, D., and Weinberg, R.A. (2011). Hallmarks of cancer: the next generation. *Cell* **144**, 646–674.
- Ikeda, Y., Sciarretta, S., Nagarajan, N., Rubattu, S., Volpe, M., Frati, G., and Sadoshima, J. (2014). New insights into the role of mitochondrial dynamics and autophagy during oxidative stress and aging in the heart. *Oxid. Med. Cell. Longev.* **2014**, e210934.
- Jakobsen, C.M., Denmeade, S.R., Isaacs, J.T., Gady, A., Olsen, C.E., and Christensen, S.B. (2001). Design, synthesis, and pharmacological evaluation of thapsigargin analogues for targeting apoptosis to prostatic cancer cells. *J. Med. Chem.* **44**, 4696–4703.
- Jiang, X., Overholzer, M., and Thompson, C.B. (2015). Autophagy in cellular metabolism and cancer. *J. Clin. Invest.* **125**, 47–54.
- Kimura, S., Noda, T., and Yoshimori, T. (2007). Dissection of the autophagosomal maturation process by a novel reporter protein, tandem fluorescent-tagged LC3. *Autophagy* **3**, 452–460.

- Korge, P., and Weiss, J.N. (1999). Thapsigargin directly induces the mitochondrial permeability transition. *Eur. J. Biochem.* 265, 273–280.
- Kroemer, G. (2015). Autophagy: a druggable process that is deregulated in aging and human disease. *J. Clin. Invest.* 125, 1–4.
- Kroemer, G., Galluzzi, L., and Brenner, C. (2007). Mitochondrial membrane permeabilization in cell death. *Physiol. Rev.* 87, 99–163.
- Lemasters, J.J., Theruvath, T.P., Zhong, Z., and Nieminen, A.-L. (2009). Mitochondrial calcium and the permeability transition in cell death. *Biochim. Biophys. Acta* 1787, 1395–1401.
- Loupakis, F., Cremolini, C., Masi, G., Lonardi, S., Zagonel, V., Salvatore, L., Cortesi, E., Tomasello, G., Ronzoni, M., Spadi, R., et al. (2014). Initial therapy with FOLFOXIRI and bevacizumab for metastatic colorectal cancer. *N. Engl. J. Med.* 371, 1609–1618.
- Mahalingam, D., Wilding, G., Denmeade, S., Sarantopoulos, J., Cosgrove, D., Cetnar, J., Azad, N., Bruce, J., Kurman, M., Allgood, V.E., and Carducci, M. (2016). Mipsagargin, a novel thapsigargin-based PSMA-activated prodrug: results of a first-in-man phase I clinical trial in patients with refractory, advanced or metastatic solid tumours. *Br. J. Cancer* 114, 986–994.
- Majumder, B., Baraneedharan, U., Thiagarajan, S., Radhakrishnan, P., Narasimhan, H., Dhandapani, M., Brijwani, N., Pinto, D.D., Prasath, A., Shanthappa, B.U., et al. (2015). Predicting clinical response to anticancer drugs using an ex vivo platform that captures tumour heterogeneity. *Nat. Commun.* 6, 6169.
- Manic, G., Obrist, F., Kroemer, G., Vitale, I., and Galluzzi, L. (2014). Chloroquine and hydroxychloroquine for cancer therapy. *Mol. Cell. Oncol.* 1, e29911.
- Ni Chonghaile, T., Sarosiek, K.A., Vo, T.-T., Ryan, J.A., Tammareddi, A., Moore, V.D.G., Deng, J., Anderson, K.C., Richardson, P., Tai, Y.-T., et al. (2011). Pretreatment mitochondrial priming correlates with clinical response to cytotoxic chemotherapy. *Science* 334, 1129–1133.
- Orrenius, S., Zhivotovsky, B., and Nicotera, P. (2003). Regulation of cell death: the calcium-apoptosis link. *Nat. Rev. Mol. Cell Biol.* 4, 552–565.
- Pinton, P., Giorgi, C., Siviero, R., Zecchini, E., and Rizzuto, R. (2008). Calcium and apoptosis: ER-mitochondria Ca<sup>2+</sup> transfer in the control of apoptosis. *Oncogene* 27, 6407–6418.
- Prevarkaya, N., Skryma, R., and Shuba, Y. (2010). Ion channels and the hallmarks of cancer. *Trends Mol. Med.* 16, 107–121.
- Prevarkaya, N., Skryma, R., and Shuba, Y. (2004). Ca<sup>2+</sup> homeostasis in apoptotic resistance of prostate cancer cells. *Biochem. Biophys. Res. Commun.* 322, 1326–1335.
- Quynh Doan, N.T., and Christensen, S.B. (2015). Thapsigargin, origin, chemistry, structure-activity relationships and prodrug development. *Curr. Pharm. Des.* 21, 5501–5517.
- Ravikumar, B., Sarkar, S., Davies, J.E., Futter, M., Garcia-Arencibia, M., Green-Thompson, Z.W., Jimenez-Sanchez, M., Korolchuk, V.I., Lichtenberg, M., Luo, S., et al. (2010). Regulation of mammalian autophagy in physiology and pathophysiology. *Physiol. Rev.* 90, 1383–1435.
- Rossi, A., Pizzo, P., and Filadi, R. (2019). Calcium, mitochondria and cell metabolism: a functional triangle in bioenergetics. *Biochim. Biophys. Acta Mol. Cell Res.* 1866, 1068–1078.
- Sætre, F., Korseberg Hagen, L., Engedal, N., and Seglen, P.O. (2015). Novel steps in the autophagic-lysosomal pathway. *FEBS J.* 282, 2202–2214.
- Sheridan, C., and Martin, S.J. (2010). Mitochondrial fission/fusion dynamics and apoptosis. *Mitochondrion* 10, 640–648.
- Sui, X., Chen, R., Wang, Z., Huang, Z., Kong, N., Zhang, M., Han, W., Lou, F., Yang, J., Zhang, Q., et al. (2013). Autophagy and chemotherapy resistance: a promising therapeutic target for cancer treatment. *Cell Death Dis.* 4, e838.
- Twig, G., Hyde, B., and Shirihai, O.S. (2008). Mitochondrial fusion, fission and autophagy as a quality control axis: the bioenergetic view. *Biochim. Biophys. Acta* 1777, 1092–1097.
- Vanden Abeele, F., Skryma, R., Shuba, Y., Van Coppenolle, F., Slomianny, C., Roudbaraki, M., Mauroy, B., Wuytack, F., and Prevarkaya, N. (2002). Bcl-2-dependent modulation of Ca<sup>2+</sup> homeostasis and store-operated channels in prostate cancer cells. *Cancer Cell* 1, 169–179.
- Wang, M., and Kaufman, R.J. (2014). The impact of the endoplasmic reticulum protein-folding environment on cancer development. *Nat. Rev. Cancer* 14, 581–597.
- Wen, S., Zhu, D., and Huang, P. (2013). Targeting cancer cell mitochondria as a therapeutic approach. *Future Med. Chem.* 5, 53–67.
- White, E. (2015). The role for autophagy in cancer. *J. Clin. Invest.* 125, 42–46.
- Winther, A.-M.L., Liu, H., Sonntag, Y., Olesen, C., le Maire, M., Soehnel, H., Olsen, C.-E., Christensen, S.B., Nissen, P., and Møller, J.V. (2010). Critical roles of hydrophobicity and orientation of side chains for inactivation of sarcoplasmic reticulum Ca<sup>2+</sup>-ATPase with thapsigargin and thapsigargin analogs. *J. Biol. Chem.* 285, 28883–28892.
- Yang, Z.J., Chee, C.E., Huang, S., and Sinicrope, F.A. (2011). The role of autophagy in cancer: therapeutic implications. *Mol. Cancer Ther.* 10, 1533–1541.
- Ying, Z., Xiang, G., Zheng, L., Tang, H., Duan, L., Lin, X., Zhao, Q., Chen, K., Wu, Y., Xing, G., et al. (2018). Short-term mitochondrial permeability transition pore opening modulates histone lysine methylation at the early phase of somatic cell reprogramming. *Cell Metab.* 28, 935–945.e5.
- Zhang, G., Frederick, D.T., Wu, L., Wei, Z., Krepler, C., Srinivasan, S., Chae, Y.C., Xu, X., Choi, H., Dimwamwa, E., et al. (2016). Targeting mitochondrial biogenesis to overcome drug resistance to MAPK inhibitors. *J. Clin. Invest.* 126, 1834–1856.
- Zhivotovsky, B., and Orrenius, S. (2011). Calcium and cell death mechanisms: a perspective from the cell death community. *Cell Calcium* 50, 211–221.
- Zuo, W., Zhang, S., Xia, C.-Y., Guo, X.-F., He, W.-B., and Chen, N.-H. (2014). Mitochondria autophagy is induced after hypoxic/ischemic stress in a Drp1 dependent manner: the role of inhibition of Drp1 in ischemic brain damage. *Neuropharmacology* 86, 103–115.

## **Supplemental Information**

### **Co-targeting Mitochondrial Ca<sup>2+</sup>**

#### **Homeostasis and Autophagy**

#### **Enhances Cancer Cells' Chemosensitivity**

**Charlotte Dubois, Artem Kondratskyi, Gabriel Bidaux, Lucile Noyer, Eric Vancauwenberghe, Valério Farfariello, Robert-Allain Toillon, Morad Roudbaraki, Dominique Tierny, Jean-Louis Bonnal, Natalia Prevarskaya, and Fabien Vanden Abeele**

## **Inventory of Supplemental Information**

Transparent methods

Supplemental Figures

Supplementary Figure Legends

Supplementary text

Supplementary references

### **Transparent methods**

**Cell culture and transfection**—Prostate cancer cell lines LNCaP and PC-3 were purchased from the American Type Culture Collection (ATCC) and cultured in RPMI-1640 medium (Gibco-Life Technologies, Grand Island, NY, USA) supplemented with 5 mM L-glutamine (Gibco-Life Technologies) and 10% fetal bovine serum (Sigma-Aldrich). Breast cancer cell lines MCF7 cells and MDA-MB-231 were cultured in Dulbecco's minimal essential medium (DMEM) and GlutaMAX (Invitrogen, Life Technologies) supplemented with 10% FCS (fetal calf serum) (Sigma-Aldrich). Stromal prostate cancer cells were obtained from and cultured in steroid free RPMI-1640 medium (Gibco-Life Technologies) supplemented with 5 mM L-glutamine (Gibco-Life Technologies), 10% FCS (Sigma-Aldrich) and 10 nM DHT. Pancreatic cancer cell line MIA-PaCa2 was purchased from the ATCC and cultured in RPMI-1640 medium (Gibco-Life Technologies) supplemented with 5 mM L-glutamine (Gibco-Life Technologies) and 10% FCS Gold (PAA Laboratories GmbH, Colbe, Germany). Hepatocarcinoma cell line Huh7 was cultured in Dulbecco's minimal essential medium (DMEM) and GlutaMAX (Invitrogen, Life Technologies) supplemented with 10% FCS (Sigma-Aldrich) in supplemented with NEAA 1X final concentration (Cambrex).



LNCaP cells were transiently transfected with mCherry-eGFP-LC3B construct using Nucleofector Technology (Lonza, Basel, Switzerland) as described by the manufacturer. Briefly, one million of cells were transfected with 2 µg of mCherry-eGFP-LC3B plasmid and seeded on tissue culture dishes with cover glass bottom (FluoroDish, FD35; World Precision Instruments, Inc., Hertfordshire, UK). Two days after plating, cells were used for treatments and subsequent confocal imaging. Tandem mCherry-GFP reporter fluorescence assay is based on the use of the pH-sensitive fluorescent tag consisting of a tandem fusion of the red, acid-insensitive mCherry and the acid-sensitive GFP. Under neutral pH, both mCherry and GFP fluoresce and colocalize indicating an autophagosome which is not fused with acidic lysosome. Alternatively, colocalization of mCherry and GFP signals could point on an amphisome or autolysosome with decreased acidification and/or impaired proteolytic degradation. In contrast, mCherry signal without GFP corresponds to an amphisome or an autolysosome with physiologically acidic interior.

siRNA cell transfection—LNCaP cells were transfected for 48 hours with siRNA (Eurogentec, Angers, France) using 6 µl Hyperfect transfection reagent (Qiagen), following the manufacturer's instructions. siRNA sequences used in these experiments are listed below:

siPERK1 5'-UAAACUAACUGCUUUCAAG-3'

siPERK2 5'-ACUAAUCGAUUGCAUUAUUG-3'

siCHOP 5'-GAACCAGCAGAGGUCACAA-3'

siATG51 5'-UAUCUCAUCCUGAUUAUAGC-3'

siATG52 5'-AUGAGCUUCAUUGCAUCC-3'

**Calcium Imaging**—Cells were plated onto 30-mm glass coverslips and grown for 3 days. Cells were loaded with 4 µM Fura-2 AM in the incubator at 37 °C for 30 min in the growth medium. Ca<sup>2+</sup> recordings were performed at 37°C by using a temperature controller associated with the imaging platform (incubator box combined with a precision air heater: LIFE IMAGING

SERVICES; Efringerstrasse 79; CH-4057 Basel; Switzerland). Recordings were performed in HBSS containing (in mM): 140 NaCl, 5 KCl, 1 MgCl<sub>2</sub>, 2 CaCl<sub>2</sub>, 0.3 Na<sub>2</sub>HPO<sub>3</sub>, 0.4 KH<sub>2</sub>PO<sub>4</sub>, 4 NaHCO<sub>3</sub>, 5 glucose and 10 HEPES adjusted to pH 7.4 with NaOH. The cells were then washed three times in HBSS. The fluorescent intensity of Fura-2 in each cell was monitored and recorded at 340 and 380 nm. To represent the variation in the intracellular free calcium concentration, the fluorescence intensity ratio represented by F<sub>340</sub>/F<sub>380</sub> was used as an indicator of changes in cytosolic Ca<sup>2+</sup> concentrations. Fluorescence was excited using an illumination DG4 system (Sutter) fitted with a xenon lamp (300 W). All recordings of Calcium fluorescence were acquired using objective 20× in the Superfluor Nikon Eclipse Ti-series inverted microscope coupled to an EMCCD camera Rolera EM-C2 (Qimaging) and processed using Metafluor 7.7.5.0 software. Typically, we measured individually between 60-80 cells per experiment and we repeated this at least 3 or 4 times and a representative figure is presented. Background fluorescence was selected as an area containing no cells and subtracted from each data point obtained during experiment. We also checked that ratio or calibrated values obtained from Ca<sup>2+</sup> imaging experiments are similar when we compared TG and ASP-8ADT treated cells.

**Apoptosis assay**—The level of apoptosis was estimated from the number of apoptotic nuclei revealed by Hoechst staining or using TUNEL assay. After 16 hr of treatment, cells were stained with In Situ Cell Death Detection Kit (TMR Red Roche). Briefly, according to the manufacturer's protocols, cells were fixed in 4% PFA/PBS (15 min, RT) and permeabilized with 0,25% Triton 100X /PBS (20 min, RT). After TdT reaction (60 min, 37°C), cells were stained with Hoechst/PBS (1/500) for 15min at RT. Staining was visualized by LSM 700 confocal imaging system. For formalin-fixed and paraffin-embedded tissues, tumor slices (6 μm) were incubated with PBS-Gelatin at 37°C in a humidified chamber. After TUNEL staining reaction (60 min, 37°C), cells were washed twice with PBS-G. Finally, cells were stained with

Hoechst/PBS (1/500) for 15 min at RT. Stainings were visualized by LSM 700 confocal imaging system.

**Electron microscopy**—Cells were cultured in a 75 cm<sup>2</sup> flask and fixed on ice with 2.5% glutaraldehyde in 0.1 M cacodylate buffer, pH 7.4 for 15 min. Cells were washed 4 times for 5 min in 0.1 M cacodylate buffer, pH 7.4. Cells were centrifuged (3min, 600g), fixed in 1% osmium tetroxide 0.1 M cacodylate buffer, pH 7.4 (15 min) and washed in 0.1 M cacodylate buffer, pH 7.4 (10 min). Pellets were stained with 2% uranyl acetate in distilled water for 15 min, dehydrated in graded acetonitrile/ water, and embedded in Epon®. The pellets were mounted on microtome supports and rapidly frozen in melting nitrogen. Ultrathin sections, of about 90–100 nm, were obtained using a Leica UC7 cryo-ultramicrotome equipped with an FC7 device. After staining with 0.5% uranyl acetate in 1.5% methyl cellulose, sections were observed on a Hitachi H600 transmission electron microscope at 75 kV accelerating voltage.

**Animals, siRNA Injection, and Tumorigenicity Assays**—Studies involving animals, including housing and care, method of euthanasia, and experimental protocols, were conducted in accordance with the local animal ethical committee in the animal house (C59-00913; protocol CEEA 202012) of the University of Sciences and Technologies of Lille, under the supervision of Dr. Lehen'kyi (59-009270). Tumor cells ( $2 \times 10^6$  cells/mouse) were injected subcutaneously in 50% (v:v) Matrigel (BD Biosciences) to 6- to 8-week-old male nude mice for PC3 (prostate) experiment and 6 to 8-week-old female nude mice for MDA-MB231 (breast) experiment, and tumors were measured every day. When tumors grew exponentially, ASP-8ADT (2  $\mu$ M, 50  $\mu$ L) diluted in PBS was injected peritumorally. CQ diluted in PBS was injected i.p. on a daily basis (50 mg/kg). Tumor volume was estimated by the following formula: (length x width<sup>2</sup>)/2.

**Subcellular fractionation**—The homogenate was prepared accordingly to the Kontès method with cells resuspended in 500  $\mu$ L of buffer (0.25 M sucrose, 1 mM EDTA, 20 mM Hepes-KOH,

pH 7.4, add anti-proteases at the end). The nuclear fraction was pelleted by centrifugation at 1000g for 10 min, two times. The light mitochondrial fraction was pelleted by centrifugation of the heavy supernatant at 15,000-17,000g for 10 min. The microsomal fraction was obtained by the centrifugation the light mitochondrial supernatant at 100,000g for 45 min. All pellets were resuspended in RIPA by gentle homogenization.

**Human tumor explant culture and treatment**—After tumor resection, tumor tissues were sectioned into ~300 µm slices using McIlwain tissue chopper. For each patient 5 ml of non-heparinized blood was collected and serum was separated at 2000g for 15 min at 4°C. Tumor tissues were confirmed by anatomopathological examination. These tumor sections were randomized and cultured in 12-well flat bottom plates coated with collagen in RPMI-1640 medium (1% kanamycine, 1% Pen/Strep, GlutaMAX) supplemented with 2% patient serum, 8% FCS (Life Technologies). Prostate tumors were treated with Docetaxel (10 nM). ASP-8ADT was used at 1 µM and CQ at 25 µM. After treatment, tumors were fixed and embedded in paraffin. The paraffin-embedded tumors were used for anatomopathological analysis (hematoxylin and eosin stain) and IHC cell death analysis.

**Ethics approval and consent to participate**—The present study was approved by Ethics Committee of GHICL Hospital, Hospital St-Philibert, Lomme, France.

**Drug combination**—To investigate the synergistic efficacy of the drug combination, the combination index (CI) and the normalized isobologram for the non-constant ratio combination design were determined according to the Chou-Talalay method using CompuSyn software version 1.0 (Chou, 2006).

**Mitochondrial membrane potential**—Briefly after overnight treatment, cells were collected and washed in PBS. The supernatant was discarded, and cells resuspended in 30 nM DiOC6(3)

reaching a cell density of  $1 \times 10^6$  cells/mL. After a 30 min incubation at  $37^\circ\text{C}$ , samples were washed in PBS, gently mixed and kept on ice. The stained cells were analyzed by measuring the fluorescence emission by flow cytometry. Briefly, cells were analyzed according to their size and granularity (the forward scatter (FSC) parameter which is relative to the size for the cell and the side scatter (SSC) parameter which correlates with the components inside the cell). We selected the main population of the cells we analyzed, and 10 000 cells were counted. Cells in medium without the fluorescent DiOC6(3) probe were used to determine a level of auto fluorescence. It shows how many cells are at each intensity of DiOC6(3). Then, we measured the intensity of DiOC6(3) of untreated cells (gate 1). We used FCCP as a positive control to induce loss of mitochondria membrane potential. DiOC6(3) histograms of healthy cells and cells with depletion of mitochondria membrane potential were overlapped to compare the intensity differences. We determined two regions of interest (R1: cells with depletion of mitochondria membrane potential and R2: healthy cells). Thus, healthy cells with high intensity in DiOC6(3) were gated in R2, while depolarized cells with lower DiOC6(3) intensity were gated in R1. We measured the increase of the percentage of cells gated in R1 following the different treatments (cells with  $\Delta\psi_m$ , % of total).

Cell-permeant, JC-1 dye (Mitoprobe, Invitrogen, Germany): JC-1 dye was added to each well on adherent cells, after an overnight treatment with the different conditions, to a final concentration of  $10 \mu\text{M}$  in RPMI medium for 30 min at  $37^\circ\text{C}$ . The stained cells were analyzed by measuring the fluorescence emission by confocal imaging (LSM 780 ZEISS). Typically, cells were loaded with JC-1 and we observed the progressive loss of red JC-1-aggregate fluorescence and a cytoplasmic diffusion of green monomer fluorescence following exposure to TG.



**Mitochondrial permeability transition pore (MPTP)**—To investigate the opening of MPTP, the calcein–cobalt technique was used according to the manufacturer specifications (Image-IT® LIVE Mitochondrial Transition Pore Assay Kit, for microscopy) (Bonora et al., 2016).

**Western Blot**—Protein samples (50 µg) were subjected to SDS-PAGE and transferred to a nitrocellulose membrane by semi-dry western blotting (Bio-Rad). The membrane was blocked in TNT buffer (Tris-HCl, pH 7.5, 140 mM NaCl, and 0.05% Tween 20) containing 5% milk for 45 min at room temperature. Then membranes were gently incubated overnight at 4°C with specific primary antibodies. Rabbit polyclonal anti-LC3B (L7543) and mouse monoclonal anti-beta Actin (A5441) were from Sigma-Aldrich (Saint-Quentin-Fallavier, France). Guinea pig anti-p62 (GP62-C) was from PROGEN Biotechnik GmbH (Heidelberg, Germany). R rabbit polyclonal anti-PARP (9542) were from Cell Signaling (Danvers, MA, USA). Polyclonal rabbit-anti-p-PERK (sc-32577), polyclonal rabbit anti-GRP78 (H-129), were from Santa Cruz Biotechnology (Heidelberg, Germany). After three 5 min washes in TNT buffer, membranes were transferred into anti-rabbit IgG horseradish peroxidase-linked secondary antibodies (Chemicon, 1/50,000) or anti-mouse horseradish peroxidase-linked secondary antibodies (Chemicon, 1/10,000) for 1 hr at room temperature. After three 15 min washes in TNT buffer, the membrane was processed for chemiluminescent detection using Supersignal West Dura chemiluminescent substrate (Pierce), according to the manufacturer's instructions. Quantifications have been done using ImageJ software. First, each relative density of band is normalized to its standard (b-actin or calnexin) to take into account loading variation. The values present in western blot figures represent the relative density of bands compared to the control condition, which will obviously have a relative density of 1.

**Time domain-fluorescence lifetime imaging microscopy (TD-FLIM)**—For live-cell imaging, cells were placed on 35mm glass bottom dishes (MatTek Corporation, USA), filled

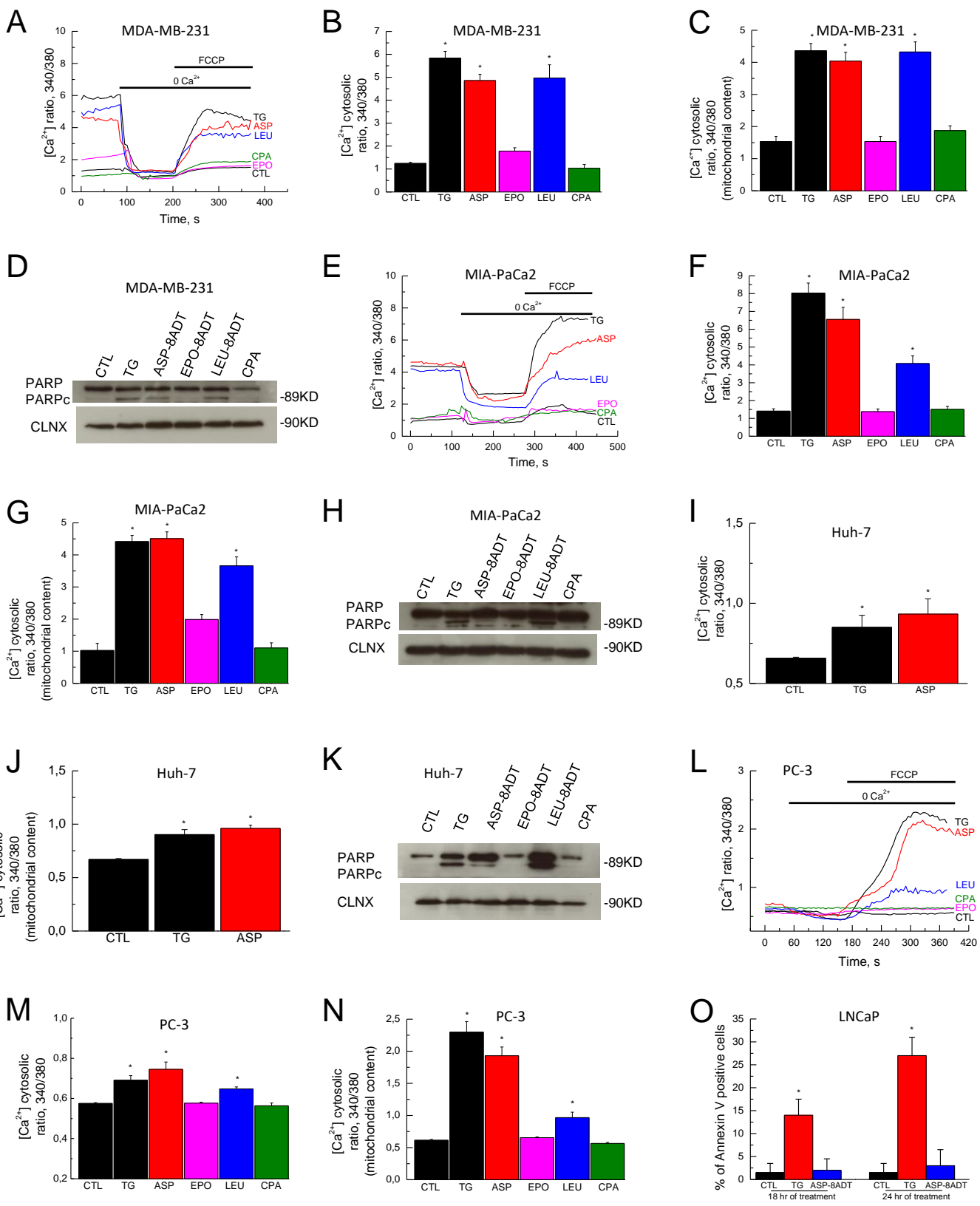
with L-15 medium without phenol red (Life technologies), and kept at 37°C using a stage incubator (Life Imaging Services, Switzerland). FLIM was performed with a Leica TCS SP5 X confocal head (Leica Microsystems, Germany) with the SMD upgrade, mounted on an inverted microscope (DMI6000, Leica Microsystems, Germany). A pulsed diode laser, PDL 800-B (PicoQuant GMBH, Germany), delivered 40 MHz repetitive rate pulses at 405 nm. The confocal pinhole was set to 1 Airy, for a 0.921  $\mu\text{m}$  optical slice. Single photon events originating from the illuminated voxel were collected through a 63x/1.2NA water-immersion lens and recorded by a TCSPC detector (HydraHarp 400; PicoQuant GMBH, Germany). Fluorescence was detected through a 483/32 single-bandpass filter (Semrock, USA) on Single Photon Avalanche Photodiodes, SPAD (MPD, Italy), set up at 256 x 256 pixels. The arrival time of single photons was measured with SymPhoTime software (PicoQuant GMBH, Germany), while images were taken with LAS AF software (Leica Microsystems, Germany). In order to obtain the best resolution for organelles, a 6-fold zoom factor was applied, giving a pixel size of 0.150  $\mu\text{m}$ . Since the statistical determination of the distribution of single photon arrival time requires at least 100 photons per pixel, 120 frames were acquired at 200Hz and summed in the final image. The TD FLIM images were analyzed with custom-made software named MAPI. Plasmid coding for the mitochondria-target Cameleon bioindicator, 4mtTM3cpv, was transfected in LNCaP cells for 36 hr and TG/ASP-8ADT treatment was carried out for 24 hr prior to an estimation of the steady-state mitochondrial  $\text{Ca}^{2+}$  concentration by the mean TD-FLIM (Time-domain-Fluorescence Lifetime Imaging Microscopy). Time-correlated single photon counting enabled us to quantify both the photon intensity and phase lifetime of the Cerulean fluorescent protein in the biosensor. Figure 1K shows that, while photon intensities of these treatments were similar, both TG and ASP-8ADT addition to the cell medium correlated to a reduced mitochondrial lifetime, thus indicating a higher proportion of the bioindicator ongoing FRET (Figures 1K and S1P). Since the latter is directly dependent on the

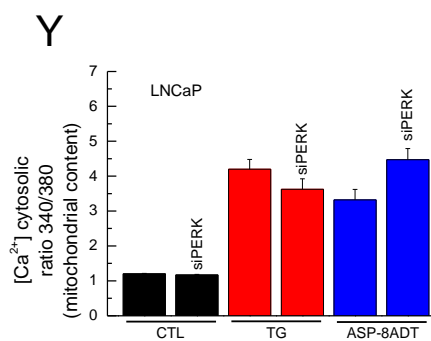
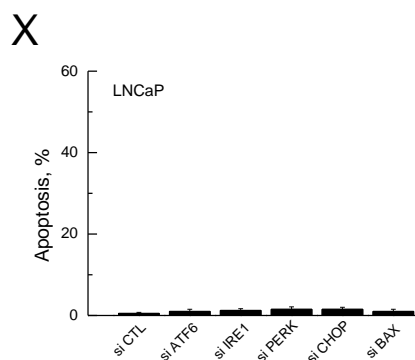
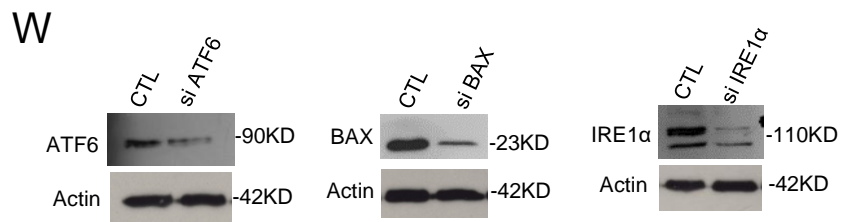
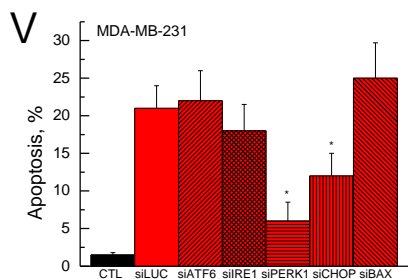
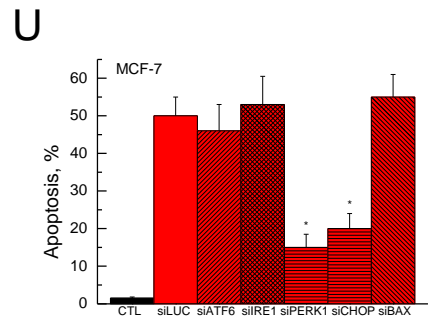
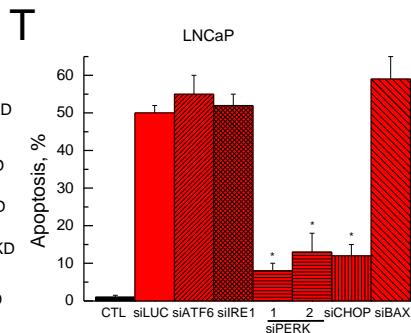
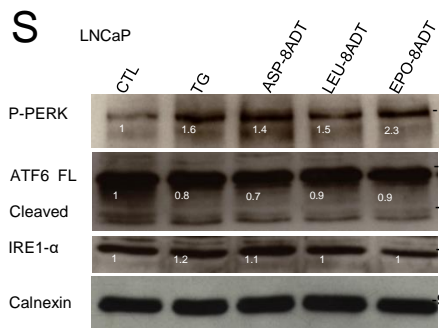
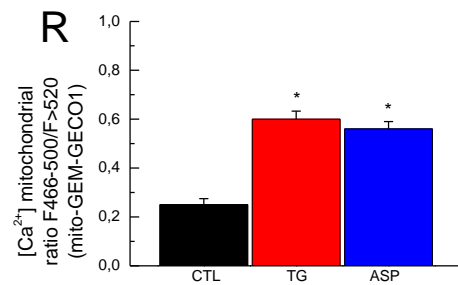
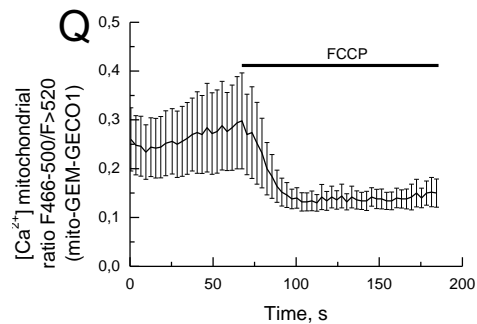
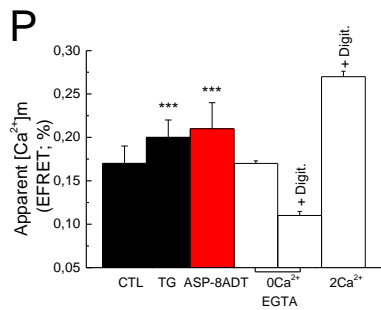
free  $[Ca^{2+}]$  in mitochondria, our results confirmed  $Ca^{2+}$  overloading in the mitochondria of LNCaP cells treated with either TG or ASP-8ADT compounds. At the end of each experiment, digitonin was used to confirm the specificity of the FRET signal (Figure S1P).

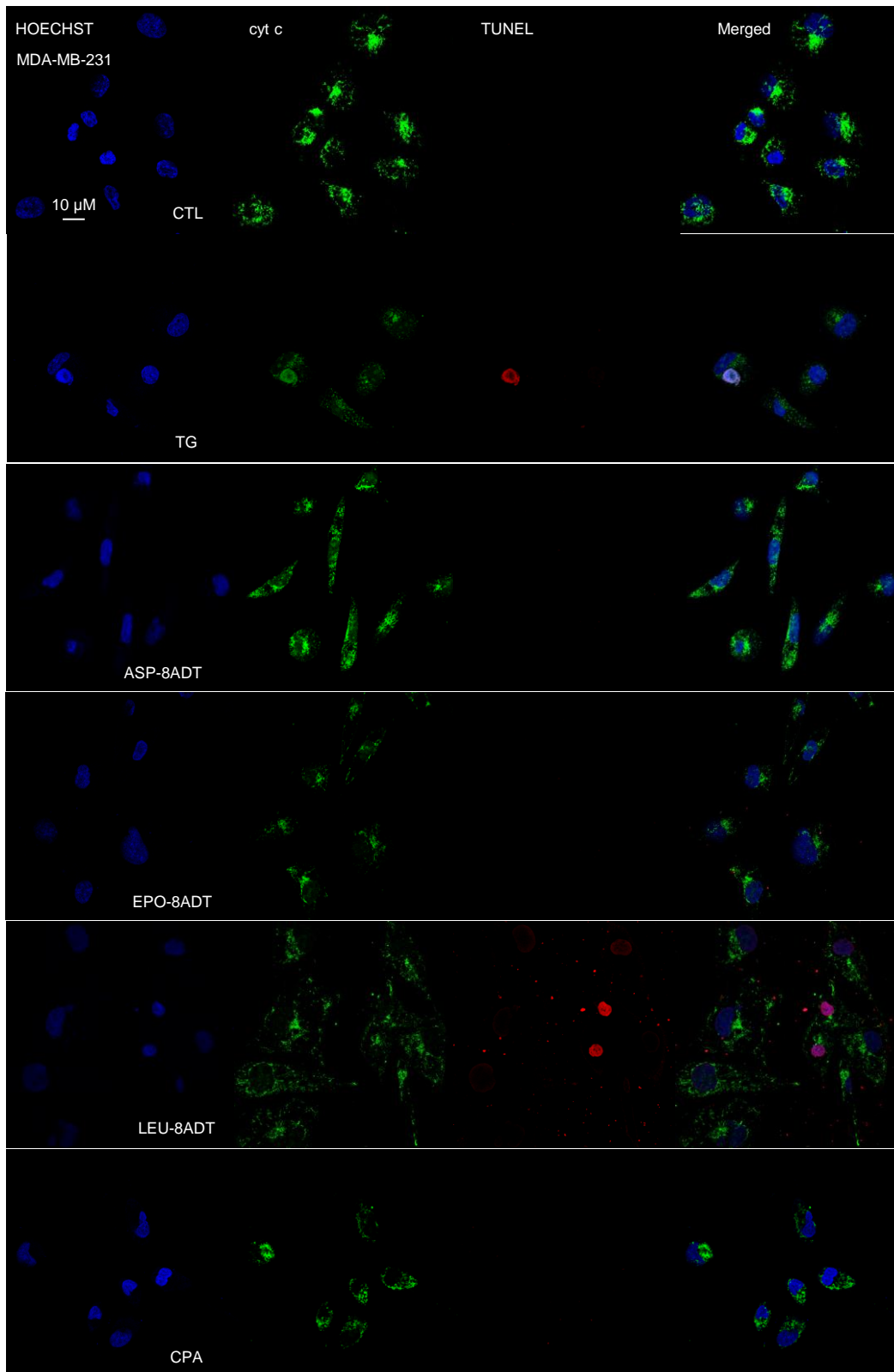
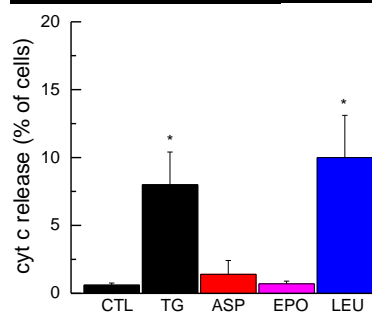
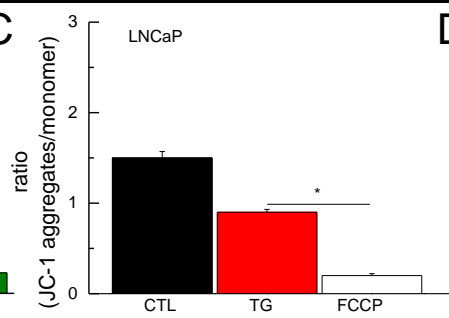
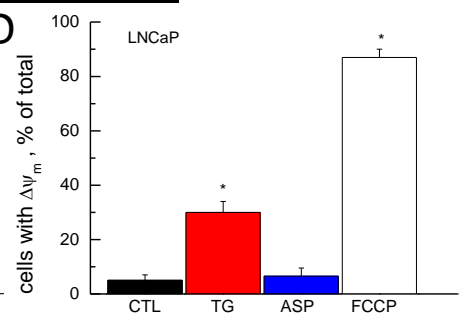
Mitochondrial  $Ca^{2+}$  content was also evaluated by the ratiometric genetically encoded  $Ca^{2+}$  probe mito-GEM-GECO1 (a gift from Robert Campbell, Addgene plasmid # 32461) expressed in LNCaP cells. The fluorescence was excited by 405 nm line on an Eclipse Ti microscope using an S Fluor 20×/0.75 NA objective lens (both from Nikon). Upon time-series  $[Ca^{2+}]$  imaging, the fluorescence then was captured at the two channels (470-500 nm and >520 nm). Images were collected through a Rolera EM-C2 charge-coupled device (CCD) camera (QImaging) controlled with Metafluor software (Molecular Devices).

**Immunocytochemistry**—Sixty percent confluent LNCaP cells were washed with PBS. After, LNCaP cells were fixed with 4% formaldehyde PBS for 15 min on ice. After three washes with PBS, cells were either incubated in PBS-gelatin (PBS with 1.2% gelatin) complemented with 0.01% Tween 20, and 100 mM glycine for 30 min at 37°C. Afterward, cells were incubated with a primary mouse monoclonal anti-cytochrome c antibody (BD Pharmigen 1:250) at 4°C overnight. After thorough washes in PBS-gelatin, the slides were treated with the corresponding Alexa Fluor 488-labeled anti-mouse IgG (1:1000) diluted in PBS-gelatin for 1 hr at room temperature. After two washes in PBS-gelatin cells are incubated with Dapi (1:250) in PBS 15 min at RT. Finally, cells were washed 3 times in PBS and slides were mounted with Mowiol and analyzed by confocal imaging (LSM 700 ZEISS).

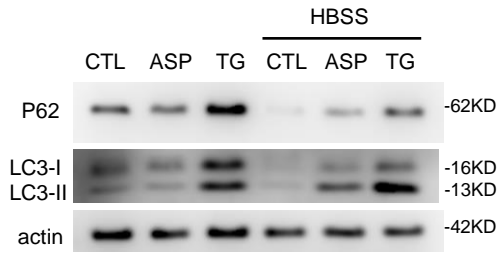
**Data analysis**—Data were analyzed and plotted using Origin 8.1 software (Microcal Software Inc.). Experiments were performed in triplicate. Results are expressed as the means  $\pm$  s.e.m. Statistical analysis was performed using Student's *t*-test (differences were considered significant when  $P < 0.05$ ).



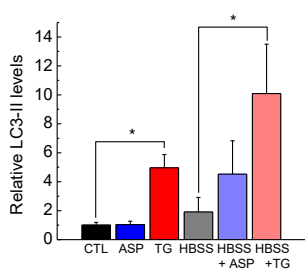


**A****B****C****D**

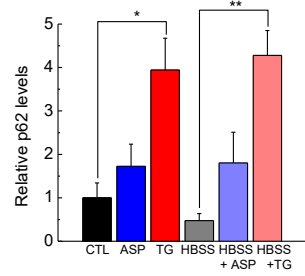
**A** PC-3



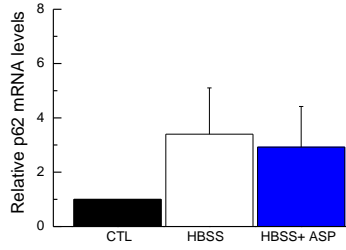
**B**



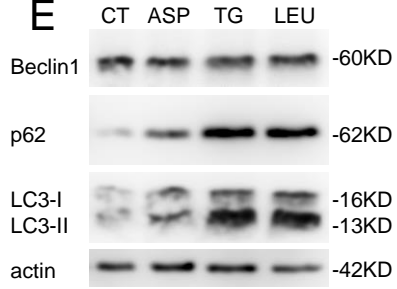
**C**

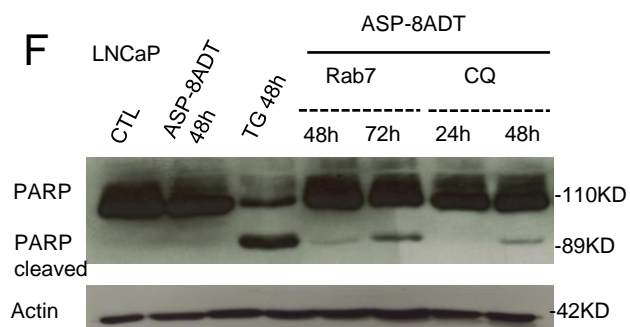
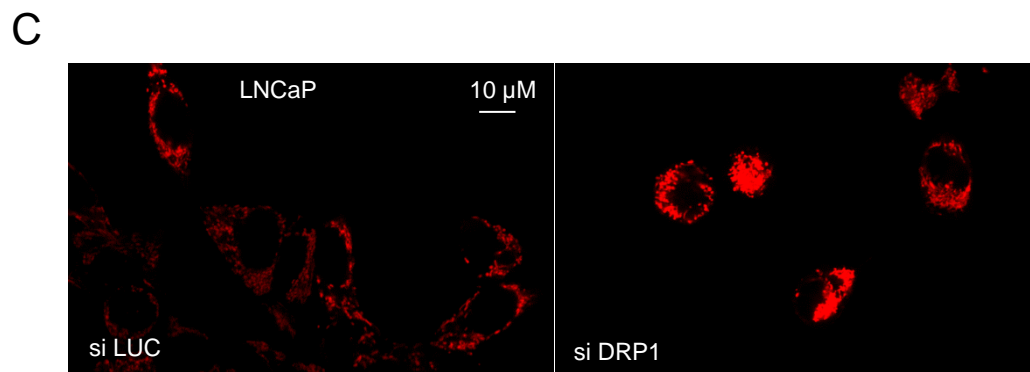
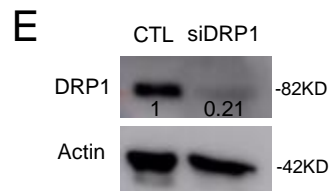
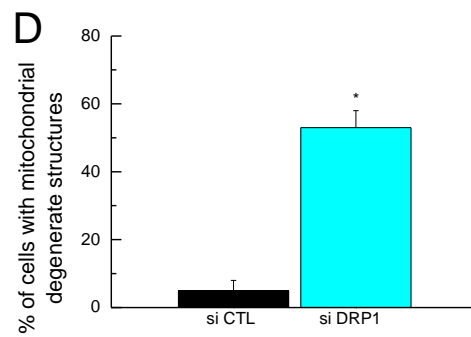
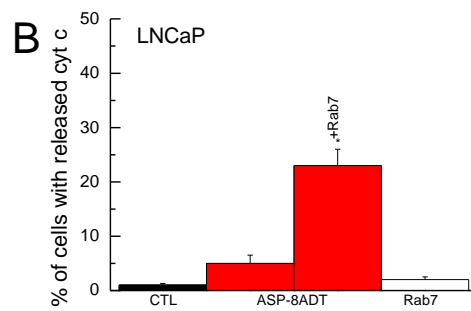
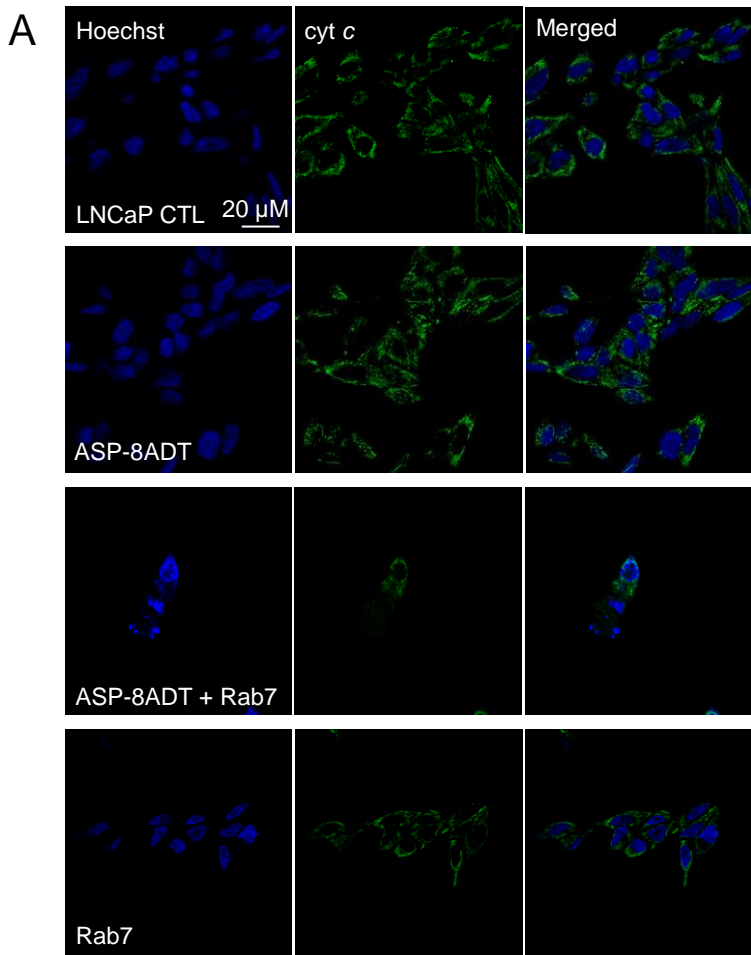


**D**

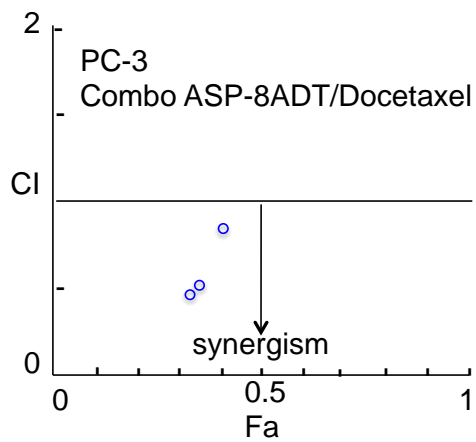
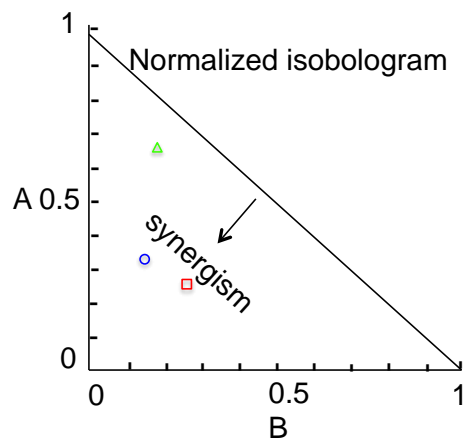


**E**

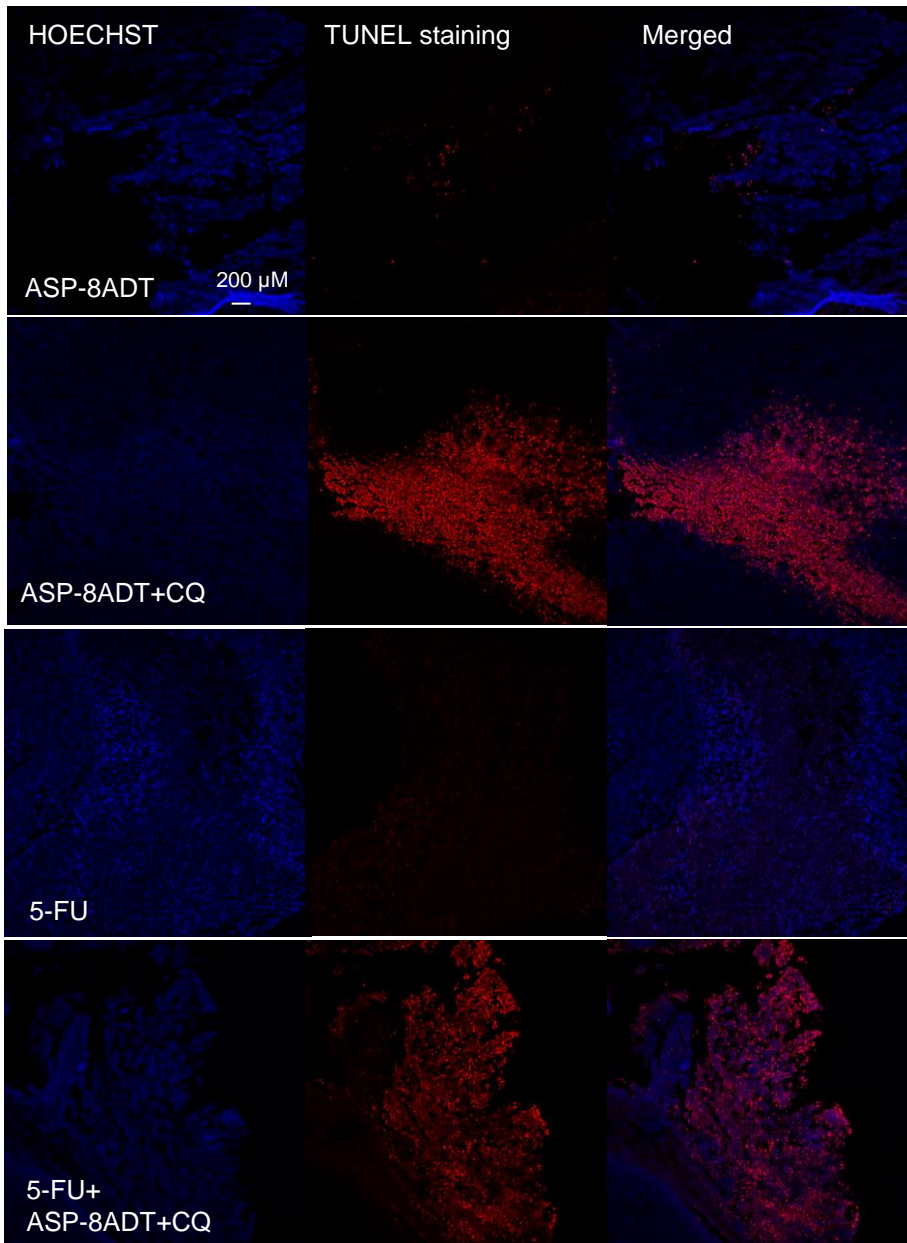






**A****B****C**

	Dose $\mu$ M ASP-8ADT (A)	Dose nM Docetaxel (B)	Effect	CI
Point 1	1.0	5.0	0.33	0.47481
Point 2	1.0	10.0	0.35	0.52363
Point 3	5.0	10.0	0.41	0.83239



## Supplementary Figure Legends

### Figure S1, Related to Figure 1

**Figure S1:** (A) Representative recordings of FCCP induced  $[Ca^{2+}]_c$  elevation in MDA-MB-231 cells subjected or not to mitochondrial  $Ca^{2+}$  overload 16 hr after SERCA pump inhibitors treatment. (B) Quantification of cytosolic  $Ca^{2+}$  content of the same set of experiment presented in (A).  $n > 50$  for each condition. (C) Quantification of mitochondrial  $Ca^{2+}$  content of the results presented in (A).  $n > 50$  for each condition. Using a mitochondrial uncoupler (FCCP), which induces the depletion of mitochondria  $Ca^{2+}$  content, we evaluated the extent of mitochondrial  $Ca^{2+}$  overload. (D) Representative Western-blot assays for cleaved and total PARP as a caspase dependent apoptosis marker in MDA-MB-231 cells after 24 hr treatment with control or TG (1  $\mu$ M) ASP-8ADT (1  $\mu$ M) EPO-8ADT (1  $\mu$ M) LEU-8ADT (1  $\mu$ M) and CPA (10  $\mu$ M). (E-N) These panels correspond to the same set of experiments presented in (A-D) but in pancreatic MIA-PaCa2 cells, hepatocarcinoma HUH-7 cells, and prostate PC-3 cells. (O) Quantification of apoptotic cells 18 hr or 24 hr after treatment with the control or the indicated drug (TG, 1  $\mu$ M; ASP-8ADT, 1  $\mu$ M) (Flow cytometric detection of apoptosis with annexin V conjugates). (P) Quantification of the results presented in Figure 1K. Digitonin was used to confirm the specificity of the FRET signal. (Q, R) Quantification of mitochondrial  $Ca^{2+}$  content by the ratiometric genetically-encoded  $Ca^{2+}$  probe mito-GEM-GECO1. FCCP was used to confirm the specificity of the  $Ca^{2+}$  probe mito-GEM-GECO1. (S) A representative Western blot of the UPR marker proteins P-PERK (phospho-PERK), ATF6 FL (Full Length), ATF6 cleaved (activated form), IRE1-alpha in LNCaP cells, 1 hr after treatment with control or the indicated drug (1  $\mu$ M). Indeed, it has been largely accepted that the prolonged depletion of ER  $Ca^{2+}$  content induces ER  $Ca^{2+}$  stress and turns on UPR response. Consequently, we investigated which actor of the UPR arms, such as PERK (protein kinase RNA-like endoplasmic reticulum kinase),

IRE1 $\alpha$  (Inositol-requiring protein 1) and ATF6 (Activating transcription factor 6) are activated or not following treatment with TG and TG analogues. Typically, ER Ca<sup>2+</sup> stress responses were examined early because they correspond to the initial cellular stress responses that could later induce or fail to induce apoptosis. In fact, we did not observe any major difference in the UPR activation after TG or TG analogues treatments and these treatments only increase the expression level of phospho-PERK suggesting that all compounds were able to induce ER Ca<sup>2+</sup> stress. (T, U, V) Quantification of apoptotic cells, as determined by Hoechst staining, 48 hr after TG-treatment (1  $\mu$ M) with control or the indicated drugs or with the indicated siRNA (24 hr, 40 nM). (W) Gene knockdown efficiency was assessed on protein level by western blot (40 nM, 24 hr). (X) Quantification of apoptotic LNCaP cells, as determined by Hoechst staining. Cells were subjected to the indicated siRNA compared to control anti-luciferase siRNA (CTL) (24 hr). (Y) Quantification of mitochondrial Ca<sup>2+</sup> content as the results presented in Figure 1C in LNCaP cells subjected to the indicated siRNA (siPERK) compared to control anti-luciferase siRNA (CTL) (24 hr). Experiments performed in triplicate. Bars represent mean  $\pm$  SEM. \*P < 0.05, \*\*\*P<0.001. Student's t test.

### **Figure S2, Related to Figure 2**

**Figure S2:** (A) TUNEL staining and subcellular distribution of *cyt c* in MDA-MB-231 cells was visualized with anti-*cyt c* antibody (green fluorescence) using a confocal microscope after 18 hr of treatment with control or the indicated drug. (B) Quantification of the results presented in (A). In untreated cells, *cyt c* displayed a brighter and punctate staining, which is in agreement with its localization within mitochondria. After apoptosis induction with TG or LEU compounds revealed by Hoechst staining, apoptotic cells, identified by chromatin condensation or nuclear fragmentation, exhibited mostly less bright and more diffuse *cyt c* staining, which is consistent with its translocation from mitochondria to cytoplasm. ASP-8ADT failed to

significantly release cyt *c*. (C) Effect of FCCP (1  $\mu$ M) on fluorescence ratio (red fluorescence due to JC-1-aggregate/green fluorescence due to JC-1 monomers). FCCP is a more potent inducer of mitochondrial membrane depolarization compared to TG. This result is in agreement with the fact that TG also induced only partial MPTP opening compared to FCCP allowing an intermediate mitochondrial  $Ca^{2+}$  overload state. (D) Quantification of cells with depolarized mitochondria, as determined by the DIOC6(3) probe. (FCCP, 1  $\mu$ M). Experiments performed in triplicate. Bars represent mean  $\pm$  SEM. \*P < 0.05, \*P<0.01, Student's t test.

### **Figure S3, Related to Figure 3**

**Figure S3:** (A) Representative Western blot of the autophagy markers protein P62 (upper panel) and LC3 I & II (middle panel) in PC-3 cells after treatment under control or starvation conditions (HBSS). Drug concentration: 1  $\mu$ M. (B) (C) Quantification of the results presented in (A). (D) Quantification of p62 mRNA levels by real-time PCR in PC-3 cells confirming that P62 protein level in ASP-8ADT treated cells did not depend on variation of transcription (E) Representative Western blot of the autophagy markers protein Beclin1, P62 and LC3 I & II in LNCaP cells after treatment with control or the indicated drug with same concentration as used in (A). To reinforce the concept that the differences between TG analogues are limited to autophagy inhibition, we also confirmed that LEU compound is also able to block autophagy, as revealed by both accumulation of P62 and LC3 II. Experiments performed in triplicate. Bars represent mean  $\pm$  SEM. \*P < 0.05, Student's t test.

### **Figure S4, Related to Figure 4**

**Figure S4:** (A) The subcellular distribution of cyt *c* was visualized with anti-cytochrome *c* antibodies (green fluorescence) using a confocal microscope after 18 hr of treatment in LNCaP cells. cyt *c* labelling is more diffuse and less bright after ASP-8ADT/Rab7 treatment. In the

other conditions, cyt c labelling was punctuated and brighter suggesting mitochondrial integrity. Nuclei were stained with Hoeschst. (B) Quantification of the results presented in (A). (C) Mitochondrial network was visualized using a confocal microscope and MitoTracker Red CMXRos staining after 24 hr of treatment in LNCaP cells. Mdivi-1 and siDRP1 treatments caused a formation of mitochondrial degenerate structures, consistent with an attenuation in mitochondrial division. Robust mitochondrial hyperfusion was observed [3,4]. (D) Quantification of the results presented in (C). (E) Gene knockdown efficiency by the specific siRNA against DRP1 was assessed on protein level by western blot (20 nM, 24 hr). (F) A representative Western blot of the apoptosis marker protein PARP and PARP cleaved from the same representative experiment shown in Figure 3D (same Actin is shown here). Experiments performed in triplicate. Bars represent mean  $\pm$  SEM. \*P < 0.05, Student's t test.

#### **Figure S5, Related to Figure 5**

**Figure S5:** (A-C) Isobologram and combination index (CI) analyses for evaluating ASP-8ADT/Docetaxel interactions in combination in PC-3 cells.

#### **Figure S6, Related to Figure 6**

**Figure S6:** Hoechst and TUNEL staining obtained from MDA-MB-231 cell xenograft tumors treated with the indicated drugs in Figure 6H.

### **Supplementary text**

**Supplementary text related to Figure 1K, S1P.** Plasmid coding for the mitochondria-target Cameleon bioindicator, 4mtTM3cpv, was transfected in LNCaP cells for 36 hr and TG/ASP-8ADT treatment was carried out for 24 hr prior to an estimation of the steady-state

mitochondrial  $\text{Ca}^{2+}$  concentration by the mean TD-FLIM (Time-domain-Fluorescence Lifetime Imaging Microscopy). Time-correlated single photon counting enabled us to quantify both the photon intensity and phase lifetime of the Cerulean fluorescent protein in the biosensor. Figure 1K shows that, while photon intensities of these treatments were similar, both TG and ASP-8ADT addition to the cell medium correlated to a reduced mitochondrial lifetime, thus indicating a higher proportion of the bioindicator ongoing FRET (Figures 1K and S1P). Since the latter is directly dependent on the free  $[\text{Ca}^{2+}]$  in mitochondria, our results confirmed  $\text{Ca}^{2+}$  overloading in the mitochondria of LNCaP cells treated with either TG or ASP-8ADT compounds. At the end of each experiment, digitonin was used to confirm the specificity of the FRET signal.

**Supplementary text related to Supplementary Figure 1L.** In normal viable cells, phosphatidylserine (PS) is located on the cytoplasmic surface of the cell membrane. However, in the intermediate stages of apoptosis, PS is translocated from the inner to the outer leaflet of the membrane, exposing PS to the external cellular environment where it can be detected. These experiments confirmed that while the remodeling on  $\text{Ca}^{2+}$  homeostasis was quite similar, compared to TG, apoptosis induced by ASP-8ADT was very modest.

**Supplementary text related to Figure 1L.** We also examined the possibility that the uncoupling between  $\text{Ca}^{2+}$  homeostasis disruption and apoptosis induction with ASP-8ADT results from impairment in reactive oxygen species (ROS) accumulation. Indeed, high levels of  $\text{Ca}^{2+}$  stimulate respiratory chain activity leading to higher amounts of reactive oxygen species (ROS). ROS can further target ER-based calcium channels leading to increased release of  $\text{Ca}^{2+}$  and further increased ROS levels. Increased ROS and  $\text{Ca}^{2+}$  load can open MPTP resulting in the release of pro-apoptotic factors (Görlach et al., 2015). Our experiments performed by flow cytometry with a fluorescent ROS probe, demonstrated that both 18 hr of treatment (the time of detection has been selected in accordance with the time course of mitochondrial  $\text{Ca}^{2+}$



overload and apoptosis induction) with TG or ASP-8ADT induce similar ROS accumulation (Figure 1L). Pyocyanin was used as a positive control. For these experiments, we typically measured between 60-80 cells per experiment and we repeated this at least 3 times. We concluded from these experiments that the uncoupling between  $\text{Ca}^{2+}$  homeostasis disruption and apoptosis induction with ASP-8ADT does not result from impairment in ROS accumulation.

**Supplementary text related to Supplementary Figure 1Q.** It has been largely accepted that the prolonged depletion of ER  $\text{Ca}^{2+}$  content also induces ER  $\text{Ca}^{2+}$  stress and turns on UPR response. This sustained stress leads eventually to cell-death induction. Surprisingly, we have demonstrated that ASP-8ADT induced the prolonged depletion of ER  $\text{Ca}^{2+}$  content without significant effect on apoptosis induction in LNCaP cells compared to TG. Consequently, we investigated which actor of the UPR arms, such as PERK (protein kinase RNA-like endoplasmic reticulum kinase), IRE1 $\alpha$  (Inositol-requiring protein 1) and ATF6 (Activating transcription factor 6) are activated or not following treatment with TG and TG analogues (1 hr, 1  $\mu\text{M}$ ). Typically, ER  $\text{Ca}^{2+}$  stress responses were examined early because they correspond to the initial cellular stress responses that could later induce or fail to induce apoptosis. In fact, we did not observe any major difference in the UPR activation after TG or TG analogues treatments and these treatments only increase the expression level of phospho-PERK suggesting that all compounds were able to induce ER  $\text{Ca}^{2+}$  stress (S1Q). Then, we used a siRNA strategy to confirm the involvement of a specific pathway activated by UPR actors in response to TG. These experiments shown that only the use of siRNA (100 nM, 24 hr before respective treatments) against PERK and CHOP leads to a decrease in apoptosis, revealing that both proteins play a crucial role (S1R-T). Concerning PERK, we confirmed the results by using two non-overlapping siRNAs (siPERK1, siPERK2) to show that results are not due to off-target effects. Gene knockdown efficiency for each siRNA has been assessed on protein level by

Western Blot (S1U). We also confirmed that siRNA treatments were not by themselves cytotoxic (S1V). The involvement of PERK and CHOP has also been confirmed in MCF-7 and MDA-MB-231 cells (S1S, T). Importantly, siRNA against BAX has no effect on TG induced apoptosis (S1R-T). Finally, we showed that siRNA against PERK has no significant effect on mitochondrial  $\text{Ca}^{2+}$  content, thereby suggesting that the protective action of PERK downregulation was not related to a decrease in mitochondrial  $\text{Ca}^{2+}$  content (S1W). These experiments confirm that mitochondrial  $\text{Ca}^{2+}$  overload alone is not enough to induce apoptosis and requires a PERK dependent pathway.

**Supplementary text related to Figure 2E, F and S2A, B.** Cyt c release from mitochondria and loss of mitochondrial membrane potential ( $\Delta\Psi_m$ ) are considered to occur subsequently to continuous pore activation. We performed immunostaining of cyt c on LNCaP and MDA-MB-231 cells. Confocal images show a close correlation between the ability of TG and LEU-8ADT to induce apoptosis and the release of cyt c (Figures 2E, F, S2A, B). In untreated cells, cyt c displayed a brighter and punctate staining, which is in agreement with its localization within mitochondria. After apoptosis induction with TG or LEU compounds revealed by Hoechst staining, apoptotic cells, identified by chromatin condensation or nuclear fragmentation, exhibited mostly less bright and more diffuse cyt c staining, which is consistent with its translocation from mitochondria to cytoplasm. However, ASP-8ADT failed to significantly release cyt c. In figure S2, cyt c immunostaining shows more puncta compared to control LNCaP cells but once again labelling is more diffuse and less bright after TG (or LEU-8ADT) treatment.

**Supplementary text related to Figure 2G, H and S2C, D.** These results raise fundamental questions. First, mitochondrial membrane potential is the driving force for mitochondrial  $\text{Ca}^{2+}$  uptake and  $\text{Ca}^{2+}$  uptake will depolarize the voltage, as observed with TG. Thus, why does the equivalent  $\text{Ca}^{2+}$  uptake not depolarize mitochondria from ASP-8ADT treated cells? In fact, a

careful reading of the literature shows that the long-term effects of such  $\text{Ca}^{2+}$  uptake by mitochondria on  $\Delta\Psi_m$  are complex. Indeed, mitochondria take up  $\text{Ca}^{2+}$  via the activity of the uniporter across the inner membrane. The influx of  $\text{Ca}^{2+}$  into the mitochondrial matrix is balanced by the activity of  $\text{Ca}^{2+}$  efflux pathways dependent of the inner membrane  $\text{Na}^+/\text{Ca}^{2+}$  and  $\text{Na}^+/\text{H}^+$  exchangers. Moreover, the presence of inorganic phosphate in the matrix of mitochondria allows mitochondria to load large amounts of  $\text{Ca}^{2+}$  without altering levels of matrix-free  $\text{Ca}^{2+}$ , since  $\text{Ca}^{2+}$  and phosphate precipitate. The  $\text{Ca}^{2+}$  buffering capacities of mitochondria enable mitochondria to buffer cytosolic  $\text{Ca}^{2+}$  whenever the cytoplasmic  $\text{Ca}^{2+}$  level rises above the set point for the balance of influx and efflux of  $\text{Ca}^{2+}$ . It is well-known that continued  $\text{Ca}^{2+}$  accumulation by mitochondria causes a drain on cellular energy, as the mitochondria need to constantly reestablish the proton gradient during long-term  $\text{Ca}^{2+}$  uptake. In accordance, our results suggest that an “equilibrium” can be achieved upon ASP-8ADT exposure compared to TG. Once again, these results highlight that another crucial factor is missing with ASP-8ADT compared to TG.

Second, how cells treated with ASP-8ADT were able to maintain mitochondrial membrane potential and have high calcein permeability? In fact, the partial MPTP opening induced by ASP-8ADT (compared to ionomycin) may explain that mitochondrial membrane potential is preserved with ASP-8ADT. Indeed, MPTP opening is intrinsically depolarizing, but we clearly showed that only partial MPTP opening occurs. Moreover, a situation with no mitochondrial  $\text{Ca}^{2+}$  overload occurred only when mitochondrial potential is totally collapsed by using FCCP as pretreatment (Figure 2D). Moreover, a careful reading of the literature showed that PTP opening in intact cells may not systematically lead to mitochondrial depolarization. Indeed, in a study published in 2009, Dumas JF et al. demonstrated that the  $\text{Ca}^{2+}$  ionophore A23187 induces like ASP-8ADT in our study mitochondrial  $\text{Ca}^{2+}$  overload, PTP opening and no depolarization of mitochondria (Dumas et al., 2009).

**Supplementary text related to Figure S3.** We also confirmed the action of ASP-8ADT and TG on autophagic flux in PC-3 prostate cancer cells and we also evaluated their action on autophagic flux in conditions of autophagy induction induced by starvation (HBSS, 2 hr) (Figures S2). These results confirmed that TG is able to block autophagy, as revealed by both accumulation of P62 and LC3 II. These effects were greatly reduced with the ASP-8ADT compound. We also confirmed by real-time PCR of P62 mRNA levels that P62 protein level in ASP-8ADT treated cells did not depend on variation of transcription (Figure S3D). To reinforce the concept that the differences between TG analogues are limited to autophagy inhibition, we also confirmed that LEU compound is also able to block autophagy, as revealed by both accumulation of P62 and LC3 II (Figure S3E). We also checked the action of ASP-8ADT, TG and LEU compounds on the cellular autophagy marker Beclin-1 (Figures S3E). Beclin 1 acts during the initiation stage of autophagy by forming the isolation membrane.

### **Supplementary references**

- Bonora, M., Morganti, C., Morciano, G., Giorgi, C., Wieckowski, M.R., Pinton, P., 2016. Comprehensive analysis of mitochondrial permeability transition pore activity in living cells using fluorescence-imaging-based techniques. *Nat. Protoc.* 11, 1067–1080. <https://doi.org/10.1038/nprot.2016.064>
- Chou, T.-C., 2006. Theoretical Basis, Experimental Design, and Computerized Simulation of Synergism and Antagonism in Drug Combination Studies. *Pharmacol. Rev.* 58, 621–681. <https://doi.org/10.1124/pr.58.3.10>
- Dumas, J.F., Argaud, L., Cottet-Rousselle, C., Vial, G., Gonzalez, C., Detaille, D., Leverve, X., Fontaine, E., 2009. Effect of transient and permanent permeability transition pore opening on NAD(P)H localization in intact cells. *J. Biol. Chem.* 284, 15117–15125. <https://doi.org/10.1074/jbc.M900926200>
- Görlach, A., Bertram, K., Hudecova, S., Krizanova, O., 2015. Calcium and ROS: A mutual interplay. *Redox Biol.* 6, 260–271. <https://doi.org/10.1016/j.redox.2015.08.010>